THE ASTROPHYSICAL JOURNAL, 350:603–630, 1990 February 20

THE VERTICAL HEIGHT OF THE HORIZONTAL BRANCH: THE RANGE IN THE ABSOLUTE MAGNITUDES OF RR LYRAE STARS IN A GIVEN GLOBULAR CLUSTER

ALLAN SANDAGE
The Observatories of the Carnegie Institution of Washington
Received 1989 February 1; accepted 1989 August 17

ABSTRACT

The observed range of apparent magnitudes of RR Lyrae variables in a given cluster is shown to be real, resulting from evolution away from the zero-age horizontal branch (ZAHB). The demonstration is made using data on periods, temperatures, and magnitudes of cluster variables in M3, M4, M15, M92, NGC 6171, NGC 6723, NGC 6981, and ω Cen by showing that in a given cluster the RR Lyrae stars that are brighter than others of the same color have longer periods by the amounts expected from the larger radii calculated as if the brighter luminosities that are observed are real, rather than caused by measuring errors. A similar result using period shifts at constant amplitude for variables in a given cluster show that the effect is not due to differential reddening.

The intrinsic HB width determined in this way varies with metallicity. In the low-metallicity clusters M15 and NGC 5053, the total HB spread is 0.2 mag, rising to $\sim$0.6 mag in metal-rich clusters such as M4. In the special case of ω Cen, the abnormally large width of 0.7 mag is caused by the combination of the two effects of evolution away from the ZAHB and the dependence of the luminosity level of the ZAHB on metallicity.

The intrinsic spread in the absolute magnitude of an ensemble of RR Lyrae stars, say in a general field, caused by the two effects just mentioned complicates their use either as distance indicators or in studies that relate the luminosity zero points of Population I Cepheids and RR Lyrae stars, say in M31 or IC 1613. In galaxies where RR Lyrae stars are found only near the limit of detection, the metallicity distribution and the incompleteness of the sampling into the RR Lyrae luminosity function must be known if the resulting bias errors are to be avoided in the inferred distances or in the determination of relative period-luminosity zero points.

Subject headings: clusters: globular — stars: horizontal-branch — stars: luminosities — stars: RR Lyrae

I. INTRODUCTION

Before the first theoretical models of the zero-age horizontal branch (ZAHB) had been invented (Faulkner 1966; Faulkner and Iben 1966; Iben and Faulkner 1968), and the evolution away from it understood (Hartwick, Härm, and Schwarzschild 1968; Iben and Rood 1970; Rood 1970; Sweigart and Gross 1976; Gingold 1976; Caloi, Castellani, and Tornambè 1978; Caputo, Castellani, and Wood 1978; Sweigart, Renzini, and Tornambè 1978; Caputo, Castellani, and Wood 1978; Sweigart, Renzini, and Tornambè 1987), it was not known from the observations whether the horizontal branch (HB) did or did not have an intrinsic vertical width. To be sure, all published color-magnitude (*C-M*) diagrams do show an intrinsic vertical spread for the HB, but systematic measuring errors that vary with distance from the cluster center because of crowding are generally large, and the corrections for them are uncertain, preventing a definitive conclusion on the reality of the HB width for most clusters.

Observational programs were begun in the late 1960s at Mount Wilson to reduce the photometric errors in a number of clusters. Many plates in each color, taken with the Mount Wilson Hooker 100 inch (2.5 m) reflector, were measured for M15 (Sandage, Katem, and Kristian 1968) and for M3 (Sandage and Katem 1982), with special emphasis on the crowding problem. The conclusion, based on the *C-M* diagrams alone, was that the HB does, indeed, have a small intrinsic width in these two clusters of about 0.2 mag at a given $B-V$ color. However, without the expectations that are born from those theories that require such an HB width due to post–ZAHB evolution, the observational results were not robust enough in themselves (because of photometric crowding) to solve the problem beyond all doubt in the 1960s.

The importance of establishing the intrinsic dispersion of M_V(RR) concerns use of RR Lyrae variables as distance indicators. If $\sigma(M)$ is large, distances will be underestimated for galaxies where the observed RR Lyrae stars are close to the detection limit (Pritchet and van den Bergh 1987; Saha and Hoessel 1987) unless bias corrections are made to the adopted absolute luminosities. This is because only the intrinsically brightest of these variables will be detected in such studies, requiring knowledge of the RR Lyrae luminosity function if the data are to be interpreted correctly. The purpose of this paper is to determine the intrinsic dispersion of M_V(RR) at fixed metallicity. In the paper that follows (Sandage 1990) we inquire into the systematic variation of the level of the ZAHB with metallicity.

The method is to use data on the periods, colors, and apparent magnitudes of the RR Lyrae stars in a number of globular clusters to address the first question. The test is to determine whether variables in a given cluster that have longer periods than others of the same color have brighter measured luminosities, as required from the $P\langle\rho\rangle^{1/2} = constant$ pulsation condition if the magnitude spreads are real.

In the next section, we set out the photometric data for HB stars obtained previously in the M3 and M15 programs just mentioned. The adopted temperature and bolometric correction scales for HB stars are given in § III. In § IV we question which type of mean color, integrated over the light cycle of the

TABLE 1

PHOTOMETRIC DATA FOR NONVARIABLE M3 HB STARS

Name (1)	r" (2)	V (3)	V^c (4)	B-V (5)	B.C. (6)	m^c_{bol} (7)	log T_e (8)	ΔV^* (9)
			150" < r < 250"					
544	205	16.68	16.72	-0.16	1.22	15.50	4.176	--
416	168	17.13	17.21	-0.14	1.04	16.17	4.146	--
100	222	17.32	17.35	-0.10	0.57	16.78	4.060	--
341	156	16.05	16.15	-0.08	0.43	15.72	4.034	--
495	163	16.07	16.17	-0.08	0.43	15.74	4.034	--
418	181	16.20	16.26	-0.07	0.39	15.87	4.023	--
153	175	16.17	16.24	-0.07	0.39	15.85	4.023	--
390	178	15.97	16.04	-0.04	0.25	15.79	3.992	0.12
126	205	16.12	16.16	-0.03	0.22	15.94	3.982	0.04
528	205	15.84	15.88	-0.02	0.18	15.70	3.972	0.20
521	178	15.87	15.94	-0.01	0.15	15.79	3.963	0.10
180	168	15.61	15.69	0.02	0.07	15.62	3.938	0.25
263	200	15.74	15.79	0.05	0.04	15.75	3.920	0.07
531	165	15.65	15.73	0.07	0.02	15.71	3.913	0.08
252	168	15.72	15.80	0.07	0.02	15.78	3.913	0.01
419	190	15.71	15.77	0.08	0.02	15.75	3.910	0.03
422	163	15.52	15.60	0.08	0.02	15.58	3.910	0.20
522	212	15.66	15.70	0.10	0.01	15.69	3.904	0.08
342	193	15.63	15.68	0.11	0.01	15.67	3.902	0.09
99	212	15.68	15.72	0.12	0.00	15.72	3.899	0.04
479	163	15.46	15.54	0.12	0.00	15.54	3.899	0.22
256	156	15.61	15.71	0.38	0.05	15.66	3.806	0.03
101	203	15.65	15.69	0.41	0.06	15.63	3.797	0.05
461	197	15.58	15.63	0.43	0.08	15.55	3.790	0.11
265	247	15.61	15.63	0.44	0.08	15.55	3.787	0.11
560	234	15.63	15.65	0.44	0.08	15.57	3.787	0.09
108	186	15.57	15.63	0.45	0.09	15.54	3.784	0.11
239	153	15.66	15.76	0.45	0.09	15.67	3.784	-0.02
117	205	15.61	15.65	0.48	0.10	15.55	3.774	0.09
171	200	15.59	15.63	0.49	0.11	15.52	3.771	0.10
498	197	15.58	15.62	0.52	0.12	15.50	3.762	0.07
141	240	15.53	15.55	0.52	0.12	15.43	3.762	0.14
303	153	15.52	15.62	0.53	0.13	15.49	3.759	0.06
306	230	15.59	15.62	0.54	0.13	15.49	3.756	0.04
189	186	15.37	15.43	0.54	0.13	15.30	3.756	0.23
351	237	15.52	15.54	0.55	0.14	15.40	3.752	0.11
139	163	15.45	15.53	0.56	0.14	15.39	3.749	0.11
499	237	15.48	15.50	0.56	0.14	15.36	3.749	0.14
488	218	15.54	15.58	0.61	0.17	15.41	3.735	-0.04
			r > 250"					
85	255	17.06	17.07	-0.21	--	--	--	--
75	252	16.32	16.33	-0.10	0.57	15.76	4.060	--
61	296	16.28	16.28	-0.06	0.34	15.94	4.013	--
105	480	15.99	15.99	-0.04	0.25	15.74	3.992	0.17
103	331	15.99	15.99	-0.03	0.22	15.77	3.982	0.13
69	299	15.94	15.94	-0.03	0.22	15.72	3.982	0.18
580	270	15.86	15.86	-0.03	0.22	15.64	3.982	0.26
344	252	15.98	15.99	-0.01	0.15	15.84	3.963	0.05
81	331	15.79	15.79	-0.01	0.15	15.64	3.963	0.25
111	408	15.84	15.84	0.00	0.12	15.72	3.954	0.16
665	586	15.81	15.81	0.00	0.12	15.69	3.954	0.19
621	452	15.97	15.97	0.00	0.12	15.85	3.954	0.03
66	282	15.79	15.79	0.01	0.10	15.69	3.946	0.17
641	623	15.79	15.79	0.02	0.07	15.72	3.938	0.15
628	455	15.78	15.78	0.02	0.07	15.71	3.938	0.16
561	259	15.78	15.79	0.02	0.07	15.72	3.938	0.15
35	386	15.76	15.76	0.02	0.07	15.69	3.938	0.18
612	328	15.77	15.77	0.03	0.05	15.72	3.931	0.13
166	440	15.59	15.59	0.04	0.04	15.55	3.924	0.29
331	302	15.73	15.73	0.04	0.04	15.69	3.924	0.15
634	506	15.76	15.76	0.05	0.03	15.73	3.920	0.10
93	353	15.71	15.71	0.05	0.03	15.68	3.920	0.15
21	390	15.60	15.60	0.05	0.03	15.57	3.920	0.26
476	375	15.71	15.71	0.07	0.02	15.69	3.913	0.10
607	420	15.73	15.73	0.07	0.02	15.71	3.913	0.08
618	423	15.69	15.69	0.07	0.02	15.67	3.913	0.12
343	480	15.76	15.76	0.08	0.02	15.74	3.910	0.04

TABLE 1—*Continued*

Name (1)	r* (2)	V (3)	V^c (4)	B-V (5)	B.C. (6)	m^c_{bol} (7)	log T_e (8)	ΔV^* (9)
17	467	15.74	15.74	0.09	0.01	15.73	3.907	0.05
58	353	15.55	15.55	0.13	0.00	15.55	3.895	0.21
595	442	15.70	15.70	0.15	-0.01	15.71	3.887	0.04
353	299	15.58	15.58	0.21	0.00	15.58	3.866	0.16
635	390	15.59	15.59	0.28	0.01	15.58	3.843	0.15
38	356	15.58	15.58	0.39	0.06	15.52	3.803	0.16
599	551	15.68	15.68	0.40	0.06	15.62	3.800	0.06
506	484	15.70	15.70	0.40	0.06	15.64	3.800	0.04
578	328	15.70	15.70	0.41	0.07	15.63	3.797	0.04
574	252	15.56	15.57	0.41	0.07	15.50	3.797	0.17
620	353	15.47	15.47	0.42	0.07	15.40	3.794	0.27
475	331	15.61	15.61	0.44	0.08	15.53	3.787	0.13
502	274	15.59	15.59	0.44	0.08	15.51	3.787	0.15
151	262	15.58	15.59	0.45	0.09	15.50	3.784	0.15
191	437	15.68	15.68	0.46	0.09	15.59	3.781	0.06
232	378	15.70	15.70	0.46	0.09	15.61	3.781	0.04
50	371	15.69	15.69	0.46	0.09	15.60	3.781	0.05
257	277	15.66	15.66	0.47	0.10	15.56	3.777	0.08
133	390	15.55	15.55	0.47	0.10	15.45	3.777	0.19
285	281	15.72	15.72	0.48	0.10	15.62	3.774	0.02
568	265	15.57	15.58	0.49	0.10	15.48	3.771	0.15
570	334	15.45	15.45	0.51	0.11	15.34	3.765	0.25
42	343	15.63	15.63	0.52	0.12	15.51	3.762	0.06
143	269	15.44	15.44	0.52	0.12	15.32	3.762	0.25
610	324	15.57	15.57	0.53	0.12	15.45	3.759	0.11
65	281	15.55	15.55	0.54	0.13	15.42	3.756	0.11
588	309	15.55	15.55	0.54	0.13	15.42	3.756	0.11
319	328	15.33	15.33	0.56	0.14	15.19	3.749	0.31
670	586	15.51	15.51	0.57	0.14	15.37	3.746	0.11
575	334	15.41	15.41	0.59	0.15	15.26	3.740	0.17
3	331	15.52	15.52	0.60	0.16	15.36	3.737	0.04
593	321	15.17	15.17	0.67	0.20	14.97	3.718	--

* Col. (9) is the magnitude difference from the lower envelope of the *C-M* diagram.

RR Lyrae variables, is to be used to obtain the appropriate temperature for the pulsation equation. In § V the *C-M* diagrams for M3 and M15 from § II are converted to bolometric magnitudes and temperatures. The different shapes of the horizontal branches of these clusters are then compared with the canonical HB theoretical models of different metallicities. In § VI the adopted temperatures are combined with observed periods for RR Lyrae variables in 10 globular clusters to test for a correlation between the observed period shifts and the observed apparent magnitudes. The positive correlation shows that the observed widths of the HBs of the program clusters are real. In § VII the values of the intrinsic width of the HB in each of the 10 clusters, together with the widths found from the nonvariable stars blueward and redward of the RR Lyrae gap, are shown to be correlated with the cluster metallicity.

In Appendix A we test whether the observed width in the *C-M* diagram could be due to differential absorption across the cluster by using the period shifts calculated at constant *amplitude*, used in previous discussions of the Oosterhoff period-shift effect (Sandage 1981*a*, *b*, 1982, hereafter S81*a*, *b* and S82). Such period shifts are independent of reddening.

Finally, the remarkable case of ω Centauri is discussed in Appendix B, where the large spread of 0.7 mag for the RR Lyrae stars and for the blue HB stars is shown again (S81*a*, *b*) to be real, presumably (Gratton, Tornambè, and Ortolani 1986) because of a combination of evolution off the ZAHB and the different ZAHB luminosities for the different metallicities present in the cluster.

II. PHOTOMETRY OF HORIZONTAL-BRANCH STARS IN M3 AND M15

Data for the *nonvariable* HB stars in M3 are set out in Table 1. These have been abstracted from the catalog given by Sandage and Katem (1982, hereafter SK) that is based on measurements of 10 plates in each of the *B* and *V* colors from plates taken with the Mount Wilson 100 inch (2.5 m) Hooker telescope. The name of the star in the SK numbering system is in column (1). Distance from the cluster center (in arcseconds) is in column (2). The magnitude from the SK catalog is in column (3), and as corrected for contamination in column (4) using adopted distance-to-center corrections given in Figure 1 of S81*b*. The estimated accuracy of these catalog magnitudes is $\sigma(V) = 0.015$ mag. The bolometric corrections in column (6) and the temperatures in column (8) are from the adopted scales discussed in § III. The apparent bolometric magnitude in column (7) is the combination of columns (4) and (6). Listed in column (9) is the magnitude difference between the observed apparent magnitude from column (4) and the lower envelope of the *C-M* diagram that is drawn in Figure 1*a*. This lower envelope is assumed to be parallel to the ZAHB, although not necessarily coincident with it in zero point because of the expected measuring errors. This possible small zero-point offset between the adopted envelope line and the true ZAHB is irrelevant because of the way we shall use the data. The *variable stars* are shown as crosses (type RR*ab*) and open circles (type RR*c*) in Figure 1*a*. The data have been corrected for con-

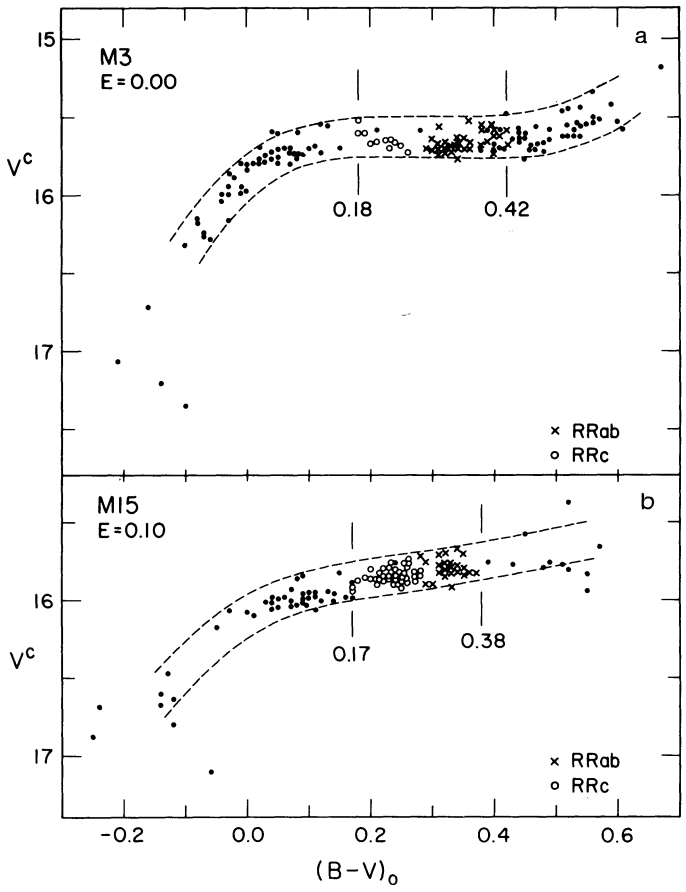

FIG. 1—Color-magnitude diagram for the horizontal branch in (*a*) M3 and (*b*) M15 from the data in Tables 1, 2, 5, and 6. The colors used for the RR Lyrae stars are $\langle B\rangle - \langle V\rangle + C(A)$ from cols. (6) and (7) of Tables 5 and 6. The envelope lines show a vertical range of $\Delta V \approx 0.2$ mag.

tamination as listed later in Table 5 in § IV, based on Table 1 of S81*b* and the measurements of Roberts and Sandage (1955).

Data for the *nonvariable* HB stars in M15 are listed in Table 2. They have been abstracted from the unpublished catalog from which the summary by Sandage, Katem, and Kristian (1968) was made. The magnitudes in column (3) are corrected for distance-to-center contamination based on Figure 3 of Sandage, Katem, and Sandage (1981, hereafter SKS). The observed colors in column (4), corrected for an adopted reddening of $E(B-V) = 0.10$, are listed in column (5). Columns (6) and (8) for the bolometric corrections and temperatures are taken from the discussion in the next section. Column (9) lists the magnitude difference between the column (3) apparent magnitude and the lower envelope to the HB CMD, whose equation is adopted to be $V(\text{envelope}) = 16.20 - 0.8(B-V)$ over the color range where there are entries in column (9). The RR Lyrae data for M15, set out later in Table 6 in § V, are based on the mean of the measurements of SKS and of Bingham *et al.* (1984, their Table 8). The data have been corrected for distance-to-center contamination.

The HB data from Tables 2 and 6 are shown in Figure 1*b*. The HB for M15 differs in shape from that in M3 in *V*-magnitudes, being more sloped than the nearly horizontal branch in M3, agreeing with the predictions of the canonical HB models for different metallicities discussed in § V.

III. ADOPTED BOLOMETRIC CORRECTIONS AND COLOR-TEMPERATURE RELATIONS FOR HORIZONTAL-BRANCH STARS

The color-temperature relations and bolometric corrections depend on surface gravity and metallicity, particularly in the temperature range of the HB. At these temperatures and surface gravities, the source of the free electrons causing the electron pressure in the stellar atmosphere changes from hydrogen ionization to the ionization of the metals as the temperature decreases at a given metallicity. This causes the color-temperature relations to be multivalued for different surface gravities (cf. Sandage 1956, Fig. 2). In addition, there is a family of such multivalued relations for different metallicities.

For the hotter HB stars we have adopted an average between the color-temperature relation determined directly for particular HB stars, summarized by Newell (1970), and those based on modern Kurucz atmospheric models in the appropriate surface gravity and metallicity ranges ($\log g = 3.0$–3.5; and [Fe/H] between -0.5 and -2.0) supplied by P. Demarque, R. Zinn, and Y.-W. Lee (1988, private communication), based on the relations given by Ciardullo and Demarque (1977). The early temperature scale by Newell (1970) is based on a series of investigations by Oke, Giver, and Searle (1962), Searle and Rodgers (1966), and Newell, Rodgers, and Searle (1969*a*, *b*). For the cooler HB stars we have adopted the temperature scales for different metallicities shown by Butler, Dickens, and Epps (1978) from calculations by Bell (unpublished) that are appropriate for the surface gravities of the RR Lyrae stars. By graphical smoothing, we have forced continuity between these two calibrations for the hot and for the cooler HB stars.

The adopted temperature and bolometric scales for the M3 and M15 HB stars are given in Table 3 for the color range in $B-V$ between -0.20 and $+0.64$ mag. We have assumed the [Fe/H] metallicities to be -1.5 and -2.0 for these clusters and have read the curves by Bell as shown by Butler, Dickens, and Epps (1978) at these metallicities. The adopted family of color-temperature relations for the relevant range of metallicities of the RR Lyrae stars is given in Figure 2. Comparison of this diagram with the data in Table 3 shows the continuity that we have made between the scales of Bell and of Newell near $B-V = 0.2$.

IV. DETERMINATION OF THE APPROPRIATE $B-V$ COLOR TO USE FOR RR LYRAE VARIABLES

Several kinds of $B-V$ colors have been used in the literature for RR Lyrae stars. The three most common are $\langle B\rangle - \langle V\rangle$, $\langle B-V\rangle$, and $(B-V)_{\text{mag}}$, where the angular brackets denote the intensity average over the light cycle and $(B-V)_{\text{mag}}$ is the mean taken over the color curve, kept in magnitude units. Preston (1961, Fig. 3) showed that $(B-V)_{\text{mag}}$ is close to that which should correspond to the temperature of the "equivalent static star."

The question of which type of mean color to use turns out to be important in the present problem. The three definitions can differ by 0.06 mag for variables with large amplitudes and asymmetric light curves. Because the amplitudes and the light-curve shapes change systematically across the RR Lyrae gap, the *slope* of the color-temperature relation that is derived from the observations depends on which definition of mean color is used.

In the previous series of papers on the Oosterhoff period effect (SKS; S81*a*, *b*, S82) we used $\langle B\rangle - \langle V\rangle$ colors, justified

TABLE 2

PHOTOMETRIC DATA FOR NONVARIABLE M15 HB STARS WITH $r > 150''$

Name (1)	r" (2)	V^c (3)	B-V (4)	$(B-V)_o$ (5)	B.C. (6)	M_{bol} (7)	Log T_e (8)	ΔV^c (9)
2163	375	16.88	-0.15	-0.25	--	--	--	--
2164	285	16.68	-0.14	-0.24	--	--	--	--
1051	161	16.60	-0.04	-0.14	1.04	15.56	4.146	--
1095	225	16.67	-0.04	-0.14	1.04	15.63	4.146	--
3156	362	16.47	-0.03	-0.13	0.90	15.57	4.123	--
1198	150	16.63	-0.02	-0.12	0.76	15.87	4.100	--
1073	326	16.80	-0.02	-0.12	0.76	16.04	4.100	--
1112	311	17.10	0.04	-0.06	0.34	16.76	4.013	--
3120	192	16.17	0.05	-0.05	0.30	15.87	4.003	-0.01
3142	188	16.07	0.07	-0.03	0.22	15.85	3.982	0.07
4017	203	16.08	0.10	0.00	0.12	15.96	3.954	0.04
4025	185	16.09	0.11	0.01	0.11	15.98	3.946	0.02
2122	210	16.01	0.13	0.03	0.09	15.92	3.931	0.09
2094	156	15.98	0.14	0.04	0.08	15.90	3.924	0.11
4069	247	16.02	0.14	0.04	0.08	15.94	3.924	0.07
4004	289	16.06	0.14	0.04	0.08	15.98	3.924	0.03
4068	291	15.99	0.15	0.05	0.07	15.92	3.920	0.09
2142	201	16.05	0.15	0.05	0.07	15.98	3.920	0.03
4019	231	15.98	0.16	0.06	0.07	15.91	3.916	0.09
3135	220	15.93	0.17	0.07	0.06	15.87	3.913	0.13
2137	179	16.01	0.17	0.07	0.06	15.95	3.913	0.05
1135	249	16.04	0.17	0.07	0.06	15.98	3.913	0.02
2150	293	15.86	0.18	0.08	0.06	15.80	3.910	0.20
3063	161	16.03	0.18	0.08	0.06	15.97	3.910	0.03
1030	188	15.84	0.19	0.09	0.05	15.79	3.907	0.21
1144	161	15.96	0.19	0.09	0.05	15.91	3.907	0.09
4098	154	15.99	0.19	0.09	0.05	15.94	3.907	0.06
1096	172	16.00	0.19	0.09	0.05	15.95	3.907	0.05
3149	320	16.03	0.19	0.09	0.05	15.98	3.907	0.02
1050	205	15.95	0.20	0.10	0.05	15.90	3.904	0.09
1020	287	15.99	0.20	0.10	0.05	15.94	3.904	0.05
4108	210	15.95	0.21	0.11	0.04	15.91	3.902	0.08
1039	311	15.97	0.21	0.11	0.04	15.93	3.902	0.06
2145	194	16.06	0.21	0.11	0.04	16.02	3.902	-0.03
1014	258	15.01	0.22	0.12	0.04	14.97	3.899	--
1027	214	16.00	0.22	0.12	0.04	15.96	3.899	0.02
1054	192	15.94	0.23	0.13	0.04	15.90	3.895	0.08
1028	189	15.96	0.24	0.14	0.04	15.92	3.890	0.05
3009	201	16.01	0.24	0.14	0.04	15.97	3.890	0.00
3087	179	15.82	0.25	0.15	0.04	15.78	3.886	0.18
1057	152	15.98	0.26	0.16	0.04	15.94	3.881	0.01
1082	168	15.88	0.27	0.17	0.03	15.85	3.877	0.10
3107	150	15.99	0.27	0.17	0.03	15.96	3.877	-0.01
4119	249	15.75	0.34	0.24	0.03	15.72	3.850	0.18
3068	311	15.75	0.49	0.39	0.10	15.65	3.795	0.06
4008	258	15.77	0.53	0.43	0.12	15.65	3.781	0.01
4094	170	15.57	0.55	0.45	0.13	15.44	3.775	0.19
2127	152	15.79	0.58	0.48	0.14	15.65	3.765	--
1001	379	15.75	0.59	0.49	0.15	15.60	3.762	--
1125	165	15.77	0.61	0.51	0.16	15.61	3.756	--
2146	218	15.36	0.62	0.52	0.16	15.20	3.753	--
1078	236	15.80	0.62	0.52	0.16	15.64	3.753	--
2003	311	15.83	0.65	0.55	0.17	15.66	3.743	--
4026	329	15.94	0.65	0.55	0.17	15.77	3.743	--
3127	285	15.65	0.67	0.57	0.18	15.47	3.738	--

NOTE.—ΔV^c in col. (9) is the difference between the lower envelope line in the C-M diagram, whose equation is $V^c(\text{envelope}) = 16.20 - 0.8(B-V)$, and the observed magnitude V, corrected for contamination, denoted by V^c in col. (3).

by the empirical fact that the correlations of this color with the other photometric parameters showed the smallest scatter. However, the slope of the period-color relation found there for the RR Lyrae stars in the six clusters studied was considerably shallower than the theoretical expectation—a fact that was ignored in my earlier analysis.

The consequence of using an incorrect slope for the color-temperature line is a progressive error in the computed period shifts that will depend on color. This is because, at a given color, the fiducial period, P_{fid} (i.e., the period on the ZAHB from which to measure the period shift defined as $\log P_{\text{obs}} - \log P_{\text{fid}}$ at fixed color), depends on the equation of this line,

TABLE 3

ADOPTED TEMPERATURE AND BOLOMETRIC CORRECTION SCALES FOR [Fe/H] = −1.5 AND −2.0

	M15		M3			M15		M3	
B-V	Log T_e	B.C.	log T_e	B.C.	B-V	Log T_e	B.C.	log T_e	B.C.
(1)	(2)	(3)	(4)	(5)	(1)	(2)	(3)	(4)	(5)
-0.20	4.260	1.68	4.260	1.68	0.24	3.850	0.03	3.856	0.00
-0.18	4.225	1.53	4.225	1.53	0.26	3.844	0.04	3.849	0.00
-0.16	4.176	1.22	4.176	1.22	0.28	3.836	0.05	3.843	0.01
-0.14	4.146	1.04	4.146	1.04	0.30	3.829	0.06	3.836	0.02
-0.12	4.100	0.76	4.100	0.76	0.32	3.822	0.07	3.829	0.02
-0.10	4.060	0.57	4.060	0.57	0.34	3.814	0.08	3.822	0.03
-0.08	4.034	0.43	4.034	0.43	0.36	3.806	0.09	3.814	0.04
-0.06	4.013	0.34	4.013	0.34	0.38	3.798	0.10	3.806	0.05
-0.04	3.992	0.25	3.992	0.25	0.40	3.791	0.10	3.800	0.06
-0.02	3.972	0.18	3.972	0.18	0.42	3.784	0.11	3.794	0.07
0.00	3.954	0.12	3.954	0.12	0.44	3.778	0.12	3.787	0.08
0.02	3.938	0.10	3.938	0.07	0.46	3.771	0.13	3.781	0.09
0.04	3.924	0.08	3.924	0.04	0.48	3.765	0.14	3.774	0.10
0.06	3.916	0.07	3.916	0.03	0.50	3.759	0.15	3.768	0.11
0.08	3.910	0.06	3.910	0.02	0.52	3.753	0.16	3.762	0.12
0.10	3.904	0.05	3.904	0.01	0.54	3.746	0.16	3.756	0.13
0.12	3.899	0.04	3.899	0.00	0.56	3.740	0.18	3.749	0.14
0.14	3.890	0.04	3.891	-0.01	0.58	3.735	0.19	3.743	0.15
0.16	3.881	0.04	3.884	-0.01	0.60	3.730	0.20	3.737	0.16
0.18	3.872	0.03	3.786	-0.01	0.62	3.724	0.21	3.732	0.17
0.20	3.865	0.02	3.869	-0.01	0.64	3.719	0.22	3.727	0.18
0.22	3.857	0.02	3.863	0.00					

NOTE.—Values from Bell (quoted in Butler, Dickens, and Epps 1978) for the RR Lyrae region, and from Newell 1970 for other HB stars.

and hence on its slope. An error in the slope will introduce a scatter in an apparent magnitude–period-shift correlation diagram in which the period shifts at all colors are combined. The size of this error will depend on how incorrect the adopted slope of the period-temperature relation may be. In this section we inquire what definition of color is appropriate so as to reconcile the slopes of the *observed* period-color relations with that which is *predicted* for the ZAHB from the pulsation theory so as to eliminate this error.

Sweigart, Renzini, and Tornambè (1987) obtain a slope of $d \log T_e/d \log P = -3.7$ for all metallicities and helium abundances (their Fig. 5) for the period-temperature relation of the ZAHB. This was found by combining the variations of luminosity and mass with temperature in their models with the pulsation equation $P = f(L, M, T_e)$ from van Albada and Baker (1971) (used later as eq. [2] in § VI). We now inquire which definition of mean color will give the slope of −3.7 for the lower envelope of the period-temperature relation of the cluster variables.

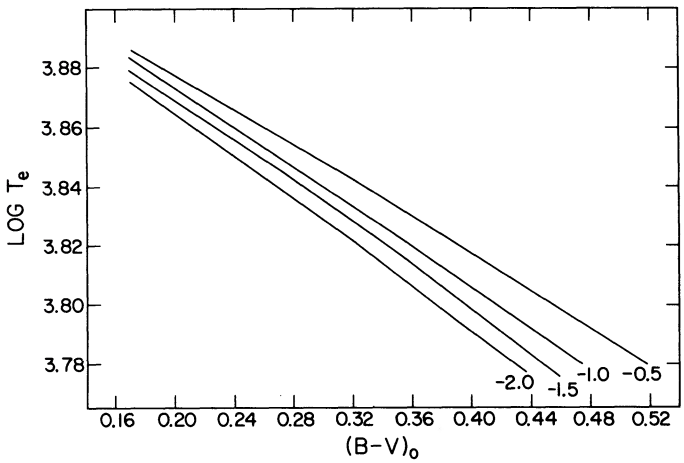

FIG. 2.—Adopted color-temperature relations for RR Lyrae stars of different metallicities from Bell, as summarized by Butler, Dickens, and Epps (1978).

Two clusters which show small scatter in their observed period-color relation are NGC 3201 (Cacciari 1984) and M3. Cacciari's data for NGC 3201 are set out in Table 4. The entries that are relevant for the discussion here are the log period in column (2), the intensity mean colors in column (4), the adopted reddening in column (5) taken from Cacciari's discussion in which a small differential reddening across the cluster is derived, giving the resulting reddening-free $\langle B\rangle - \langle V\rangle$ color in column (6). Similar data for M3, taken from Table 1 of S81*b*, are set out in Table 5. The log of the period is given in column (2). The observed mean $\langle B\rangle - \langle V\rangle$ color is given in column (5).

The period-color relation for NGC 3201 from Table 4 is shown in Figure 3. The temperature scale in Figure 3*a*, called $T_e(2)$ in SKS and in S81*b* and S82, is obtained by using $\langle B\rangle - \langle V\rangle$ colors and the color-temperature calibration discussed in § III. The drawn line is the lower envelope to the M3 data, adopted as fiducial from Figure 4, fixed with the slope of −3.7. Clearly, the $\langle B\rangle - \langle V\rangle$ color system in Figure 3*a* fails to produce the required slope. As mentioned earlier, the same failure had been found previously by SKS, S81*b*, and S82 but was ignored. From what is now to be discussed, there is no question that the incorrect slope found there resulted in use of the wrong type of color, $\langle B\rangle - \langle V\rangle$, to represent the "equivalent static star." This is seen by the following procedure and comparison.

In Figure 3*b* we have forced the data to the envelope line at each temperature by applying an empirical correction that

TABLE 4

PHOTOMETRIC PARAMETERS FOR RR LYRAE STARS IN NGC 3201

Star (1)	log P (2)	A_B (3)	<B>-<V> (4)	E (5)	[<B>-<V>]^c (6)	$(B\text{-}V)^o_{st}$ (7)	$\log T_e^{st}$ [a] (8)	$\log L/M^{0.81}$ (9)	V_o (10)	$\Delta\log P(A)^b$ (11)	$\Delta\log P(T_e)^c$ (12)
1	-0.218	1.06	0.61	0.23	0.38	0.40	3.799	1.792	14.10	0.054	0.015
2	-0.274	1.35	0.53	0.21	0.32	0.36	3.814	1.788	14.16	0.035	0.015
3	-0.222	0.90:	0.66	0.25	0.41	0.42	3.791	1.754	14.11	0.029	-0.018
4	-0.201	1.28	0.59	0.21	0.38	0.42	3.791	1.779	14.20	0.099	0.003
6	-0.280	1.36	0.49:	0.18	0.31:	0.35:	3.818	1.797	14.20	0.030	0.024
7	-0.200	0.63	0.58	0.18	0.40	0.40	3.799	1.814	14.14	0.016	0.033
8	-0.202	0.64	0.59	0.20	0.39	0.39	3.803	1.828	14.17	0.016	0.046
9	-0.278	1.30	0.55	0.21	0.34	0.38	3.806	1.750	14.10	0.025	-0.019
10	-0.272	1.37	0.56	0.22	0.34	0.38	3.806	1.757	14.20	0.040	-0.013
11	-0.524	0.66	0.47	0.25	0.22	0.22	3.863	--	14.23	--	--
12	-0.305	1.58:	0.50:	0.21	0.29:	0.35:	3.818	1.767	14.12	0.034	-0.001
13	-0.240	1.10	0.58	0.21	0.37	0.39	3.803	1.783	14.13	0.037	0.008
14	-0.293	1.38	0.59	0.27	0.32	0.36	3.814	1.765	14.13	0.020	-0.004
15	-0.272	1.36	0.47	0.18	0.29	0.33	3.825	1.836	14.13	0.038	0.058
16	-0.579	0.43	0.36	0.19	0.17	0.17	3.879	--	14.16	--	--
19	-0.280	1.45	0.52	0.21	0.31	0.36	3.814	1.781	14.08	0.042	0.009
20	-0.276	1.43	0.51	0.21	0.30	0.35	3.818	1.802	14.08	0.043	0.028
21	-0.247	1.13	0.57	0.21	0.36	0.38	3.806	1.787	14.19	0.034	0.012
22	-0.218	0.99	0.58	0.21	0.37	0.38	3.806	1.821	14.06	0.045	0.041
24	-0.230	1.00	0.57:	0.20	0.37:	0.39:	3.803	1.795	14.05	0.034	0.018
25	-0.288	1.40:	0.46:	0.18	0.28:	0.33:	3.825	1.817	14.21	0.028	0.042
26	-0.245	1.16	0.62	0.26	0.36	0.39	3.803	1.777	14.13	0.040	0.003
29	-0.276	1.22:	0.53:	0.21	0.32:	0.35:	3.818	1.802	14.16	0.016	0.028
30	-0.287	1.48	0.45	0.16	0.29	0.34	3.822	1.805	14.19	0.039	0.031
31	-0.284	1.55:	0.55:	0.25	0.30:	0.36:	3.814	1.776	14.06	0.051	0.005
32	-0.251	1.58:	0.51:	0.21	0.30:	0.36:	3.814	1.815	14.14	0.088	0.038
34	-0.330	1.50	0.45	0.20	0.25	0.31	3.832	1.796	14.14	-0.002	0.025
35	-0.211	0.85:	0.57:	0.19	0.38:	0.39:	3.803	1.817	14.17	0.034	0.037
37	-0.239	0.97	0.53	0.18	0.35	0.36	3.814	1.829	14.16	0.021	0.050
40	-0.192	0.49	0.66	0.22	0.44	0.44	3.783	1.757	14.18	0.006	-0.018
43	-0.170	0.65	0.57	0.18	0.39	0.39	3.803	1.866	14.11	0.049	0.078
46	-0.265	1.38	0.51	0.21	0.30	0.34	3.822	1.832	14.11	0.048	0.053
48	-0.467	0.54	0.47	0.21	0.26	0.26	3.849	--	14.10	--	--
49	-0.235	1.16:	0.56:	0.22	0.34:	0.37:	3.810	1.818	14.06	0.050	0.039
54	-0.255	1.20	0.60	0.26	0.34	0.37	3.810	1.794	14.09	0.035	0.019
56	-0.229	1.09	0.62	0.23	0.39	0.41	3.795	1.763	14.22	0.047	-0.011
57	-0.227	0.90	0.60:	0.22	0.38:	0.39:	3.803	1.798	14.21	0.024	0.021
58	-0.206	0.54	0.61	0.21	0.40	0.40	3.799	1.807	14.22	-0.001	0.027
59	-0.286	1.47	0.45	0.17	0.28	0.33	3.825	1.819	14.15	0.039	0.044
60	-0.298	1.57	0.39	0.13	0.26	0.32	3.829	1.821	14.20	0.040	0.046
64	-0.282	1.38	0.46	0.17	0.29	0.33	3.825	1.824	14.13	0.031	0.048
67	-0.484	0.56	0.43	0.19	0.24	0.24	3.856	--	14.12	--	--
69	-0.291	1.54:	0.45:	0.18	0.27:	0.33:	3.825	1.813	14.20	0.043	0.039
71	-0.221	0.96:	0.57	0.20	0.37	0.38	3.806	1.818	14.10	0.038	0.038
73	-0.284	1.50	0.52	0.22	0.30	0.36	3.814	1.776	14.06	0.044	0.005
83	-0.263	1.57	0.54	0.23	0.31	0.37	3.810	1.784	14.11	0.075	0.011
84	-0.289	1.32:	0.52:	0.21	0.31:	0.35:	3.818	1.786	14.17	0.016	0.015

NOTE.—From data of Cacciari 1984.

[a] Col. (8) uses the [Fe/H] = −1.5 color-temperature relation.

[b] Δ log $P(A_B)$ in col. (11) is relative to M3 lower envelope line (ZAHB) of log $P = -0.129A_B - 0.135$.

[c] Δ log $P(T_e)$ in col. (12) is relative to M3 lower envelope line (ZAHB) of log $P = -3.70 \log T_e + 13.823$.

depends on the light-curve amplitude, called $\Delta C(A)$, to the observed $\langle B\rangle - \langle V\rangle$ color. Because amplitude varies systematically and monotonically with color across the RR Lyrae strip, this amplitude correction to the colors also varies progressively with temperature, permitting the *systematic* change of the observed slope in Figure 3 to occur when the amplitude correction to the colors is applied.

A similar determination of the amplitude correction to $\langle B\rangle - \langle V\rangle$ colors was made from the RR Lyrae data for M3 in Figure 4 using data from Table 5. The lower panel shows the color-temperature relation found by applying the same $\Delta C(A)$ correction to the M3 data as that for NGC 3201. The correction, determined in this way, is shown in Figure 5. It reaches 0.06 mag in color for a light-curve amplitude of 1.6 mag.

A semitheoretical justification for Figure 5 comes from Preston's (1961) calculation of how to integrate the color curve properly over the RR Lyrae light cycle. Inspection of Preston's Figure 1 shows that the curve in Figure 5 here is closely the same as his *calculated* difference between $\langle B\rangle - \langle V\rangle$ and $(B-V)_{\rm mag}$ as a function of amplitude, supporting his conclusion that $(B-V)_{\rm mag}$ is the correct color for the equivalent "static star." In view of the agreement between Figure 5 and Preston's Figure 1, we use $\langle B\rangle - \langle V\rangle + \Delta C(A)$ colors in the following discussion.

TABLE 5

DATA FOR RR LYRAE STARS IN M3

Star (1)	log P (2)	A_B (3)	<V>[c] (4)	[<B>-<V>][c] (5)	$(B-V)^c_{st}$ (6)	m/bol (7)	log $T_{e,st}$[a] (8)	logL/M[0.81] (9)	ΔlogP(A)[b] (10)	ΔlogP(T_e)[c] (11)	ΔV[d] (12)
1	-0.283	1.33	15.67	0.28	0.32	15.65	3.829	1.839	0.024	0.061	0.07
6	-0.289	1.21	15.77	0.31	0.34	15.74	3.822	1.803	0.002	0.029	-0.03
9	-0.266	1.42	15.69	0.28	0.33	15.67	3.825	1.843	0.052	0.064	0.05
12c	-0.498	0.62	15.67	0.20	0.20	15.68	3.869	--	--	--	0.07
16	-0.291	1.46	15.72	0.28	0.33	15.70	3.825	1.813	0.032	0.039	0.02
18	-0.287	1.30	15.71	0.31	0.35	15.68	3.818	1.789	0.016	0.017	0.03
19	-0.199	0.47	15.69	0.42	0.42	15.62	3.791	1.782	-0.003	0.005	0.05
21	-0.288	1.28	15.70	0.30	0.34	15.67	3.822	1.804	0.012	0.030	0.04
24	-0.178	0.85	15.58	0.39	0.40	15.52	3.799	1.840	0.067	0.055	0.16
25	-0.319	1.42	15.74	0.26	0.31	15.72	3.832	1.809	-0.001	0.036	0.00
26	-0.223	1.35	15.63	0.29	0.34	15.60	3.822	1.882	0.086	0.095	0.11
27	-0.237	0.94	15.70	0.37	0.38	15.65	3.806	1.799	0.019	0.022	0.04
34	-0.253	0.59	15.68	0.35	0.35	15.65	3.818	1.829	-0.042	0.051	0.06
36	-0.263	1.33	15.67	0.27	0.31	15.65	3.832	1.875	0.044	0.092	0.07
37c	-0.486	0.61	15.66	0.24	0.24	15.66	3.856	--	--	--	0.08
40	-0.258	1.27	15.70	0.31	0.34	15.67	3.822	1.840	0.041	0.060	0.04
46	-0.212	0.68	15.72	0.40	0.40	15.66	3.799	1.799	0.011	0.021	0.02
48	-0.202	0.66	15.57	0.39	0.39	15.52	3.803	1.828	0.018	0.046	0.17
51	-0.234	1.18	15.69	0.32	0.35	15.65	3.818	1.852	0.053	0.070	0.05
55	-0.276	1.42	15.68	0.29	0.34	15.65	3.822	1.819	0.042	0.042	0.06
56c	-0.482	0.65	15.64	0.23	0.23	15.64	3.860	--	--	--	0.10
60	-0.150	0.73	15.55	0.38	0.38	15.50	3.806	1.902	0.079	0.109	0.19
64	-0.218	0.95	15.67	0.35	0.36	15.63	3.814	1.854	0.040	0.071	0.07
65	-0.175	1.16	15.52	0.33	0.36	15.48	3.814	1.906	0.110	0.114	0.22
71	-0.260	1.11	15.73	0.30	0.32	15.71	3.829	1.867	0.018	0.084	0.01
72	-0.341	1.63	15.69	0.25	0.32	15.67	3.829	1.770	0.004	0.003	0.05
74	-0.308	1.47	15.71	0.25	0.30	15.69	3.836	1.838	0.017	0.062	0.03
75	-0.503	0.59	15.70	0.23	0.23	15.70	3.860	--	--	--	0.04
83	-0.300	1.42	15.68	0.30	0.35	15.65	3.818	1.773	0.018	0.004	0.06
84	-0.225	0.94	15.67	0.39	0.40	15.61	3.799	1.784	0.031	0.008	0.07
85	-0.499	0.64	15.52	0.18	0.18	15.53	3.876	--	--	--	0.22
90	-0.286	1.38	15.68	0.32	0.36	15.64	3.814	1.773	0.027	0.003	0.06
93	-0.220	0.97	15.65	0.38	0.39	15.60	3.803	1.806	0.040	0.028	0.09
94	-0.281	1.39	15.70	0.25	0.29	15.68	3.839	1.883	0.033	0.100	0.04
96	-0.302	1.49	15.56	0.26	0.31	15.54	3.832	1.829	0.025	0.053	0.18
105	-0.541	0.39	15.60	0.18	0.18	15.61	3.876	--	--	--	0.14
107	-0.510	0.67	15.66	0.21	0.21	15.66	3.866	--	--	--	0.08
108	-0.284	1.36	15.71	0.28	0.32	15.69	3.829	1.838	0.026	0.060	0.03
119	-0.286	1.48	15.64	0.25	0.30	15.62	3.836	1.865	0.040	0.084	0.10
120	-0.194	0.56	15.66	0.40	0.40	15.60	3.799	1.821	0.013	0.039	0.08
124	-0.124	0.42	15.57	0.40	0.40	15.51	3.799	1.904	0.065	0.109	0.17
125	-0.456	0.53	15.68	0.25	0.25	15.68	3.853	--	--	--	0.06
126	-0.458	0.52	15.73	0.26	0.26	15.73	3.849	--	--	--	0.01
140	-0.477	0.53	15.65	0.23	0.23	15.65	3.860	--	--	--	0.09
c	-0.542	0.16	15.60	0.19	0.19	15.61	3.872	--	--	--	0.14
I-42	-0.038	0.14	15.58	0.42	0.42	15.51	3.791	1.973	--	0.166	0.16
I-100	-0.001	0.15	(15.60)	0.41	0.41	(15.54)	3.795	2.034	--	0.218	0.14

[a] The temperatures in col. (8) are from the [Fe/H] = −1.5 color-temperature relation.
[b] Δ log $P(A_B)$ in col. (10) is from the ZAHB lower envelope of log $P = -0.129A_B - 0.135$.
[c] Δ log $P(T_e)$ in col. (11) is from the ZAHB lower envelope of log $P = -3.70 \log T_e + 13.823$.
[d] ΔV in col. (12) is from the *C-M* diagram lower envelope at $V^c = 15.75$.

V. COMPARISON OF THE OBSERVED AND THEORETICAL HORIZONTAL BRANCHES FOR M3 AND M15

The photometric data for M3 from Tables 1 and 5 are plotted in Figure 6*a*. The temperatures in column (8) of both Table 1 and Table 5 and the listed bolometric magnitudes are plotted in Figure 6*b*. Similar data for M15 are shown in Figure 7, taken from Tables 2 and 6. The data in Table 6 that are required here are (1) the "static star" color in column (6), (2) the reddening-free static color in column (7) obtained by applying $E(B-V) = 0.10$ (Sandage 1969) to column (6), and (3) the bolometric apparent magnitudes and the temperatures in columns (8) and (9).

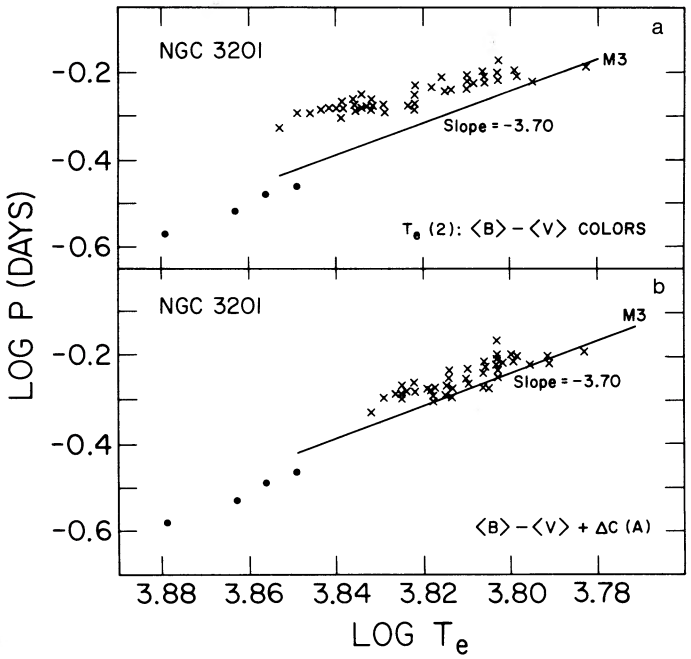

FIG. 3.—The color-temperature test. Period-temperature relation for the variables in NGC 3201. The colors are from cols. (4) and (7) of Table 4, and the temperature calibration is from Fig. 2 using [Fe/H] = −1.5. The lower envelope, fixed with a slope of −3.7, is adopted from Fig. 4 for the M3 variables. This envelope is used as a fiducial from which the Δ log $P(T_e)$ value for any variable is read as the vertical deviation.

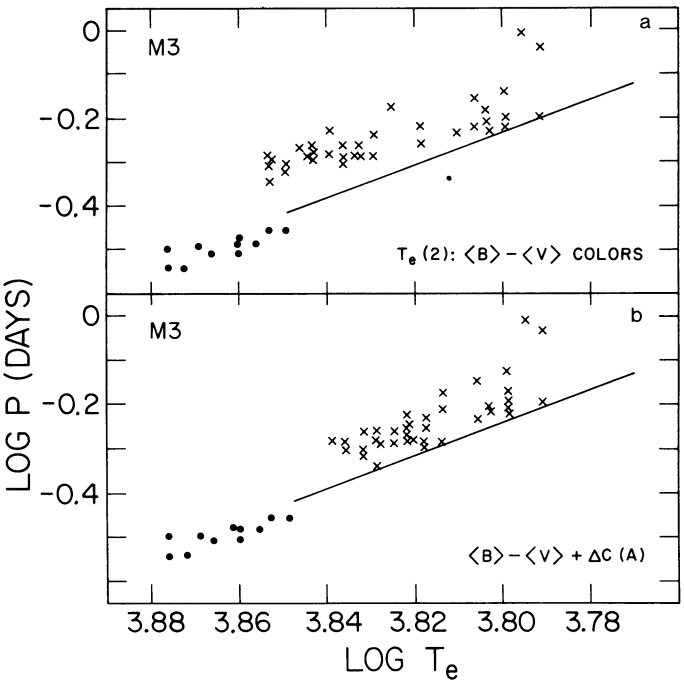

FIG. 4.—The color-temperature test. Period-temperature relation for the variables in M3 from data in Table 5 using the two types of colors in cols. (5) and (6). The slope of the lower envelope line has been fixed at −3.7. Type *c* variables are shown as filled circles, and the *ab* types are shown as crosses.

Figures 6*b* and 7*b* are set out again for comparison in the (m_{bol}, log T_e)-diagram in Figure 8. The evident difference of slope between the M3 and the M15 horizontal branches is predicted by the HB models of Sweigart and Gross (1976, hereafter SG) for different metallicities at fixed helium abundance.

The feature of these models which we need here (the slope of the ZAHB) has been confirmed by all the more recent calculations of ZAHB loci (cf. Sweigart, Renzini, and Tornambè 1987; Seidel, Demarque, and Weinberg 1987; Dorman, VandenBerg, and Laskarides 1989). The dashed lines in Figure 8 show the SG ZAHB models for $Y = 0.25$ for [Fe/H] = −1.5 and −2.0, drawn by eye as the lower envelopes to the HB distributions for the two clusters. In the RR Lyrae star region, the slopes of the theoretical curves are $d \log L/d \log T_e = -0.54$ and −0.96 for M3 and M15, respectively. The excellent agreement of these slopes with the observations shows that these early canonical SG ZAHB models are reliable in this particular detail—an important point because the same ZAHB models themselves cannot explain the period-shift problem (cf. Sweigart, Renzini, and Tornambè 1987; Buonanno, Corsi, and Fusi Pecci 1988 for reviews) for the RR Lyrae stars in clusters of different metallicities, *unless* the helium abundance is anticorrelated with the metallicity, or unless the alternate explanation given by Lee, Demarque, and Zinn (1988, 1990, hereafter collectively LDZ) is correct. In their view, *no* RR Lyrae stars in low-metallicity clusters (e.g., M92) exist on the ZAHB. They suppose that those stars that exist redward of the RR Lyrae gap have evolved from bluer ZAHB positions along tracks that make the observed RR Lyrae stars (*all being non–ZAHB*) both brighter and less massive than the ZAHB model stars of the same T_e, giving, in fact, a period shift at *constant Y* even though the *ZAHB* models predict none (Sweigart, Renzini, and Tornambè 1987). A more complete discussion of the LDZ analysis is set out in the paper that follows.

VI. PERIOD-SHIFT–MAGNITUDE RELATIONS RELATIVE TO THE ZAHB FOR RR LYRAE VARIABLES IN 10 CLUSTERS

We now demonstrate that the observed period at *fixed temperature* relative to the period on the lower envelope fiducial period-temperature line is correlated with the *observed apparent magnitude*. This correlation is, of course, required if the apparent magnitude spread of the RR Lyrae stars in a given cluster is real rather than due to measuring errors. To visualize

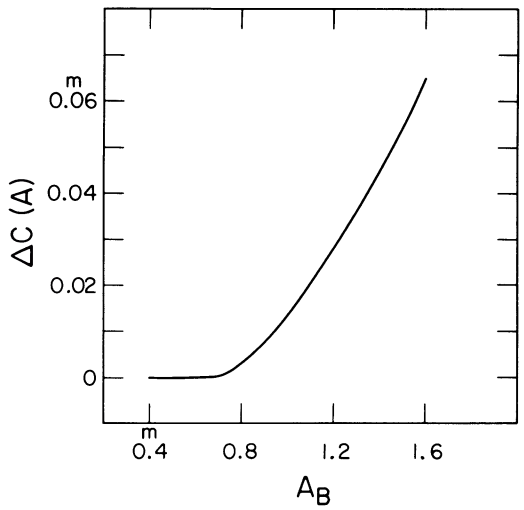

FIG. 5.—Correction to $\langle B \rangle - \langle V \rangle$ colors as a function of blue-light amplitude to obtain "static star" colors that are appropriate for use in the pulsation equation.

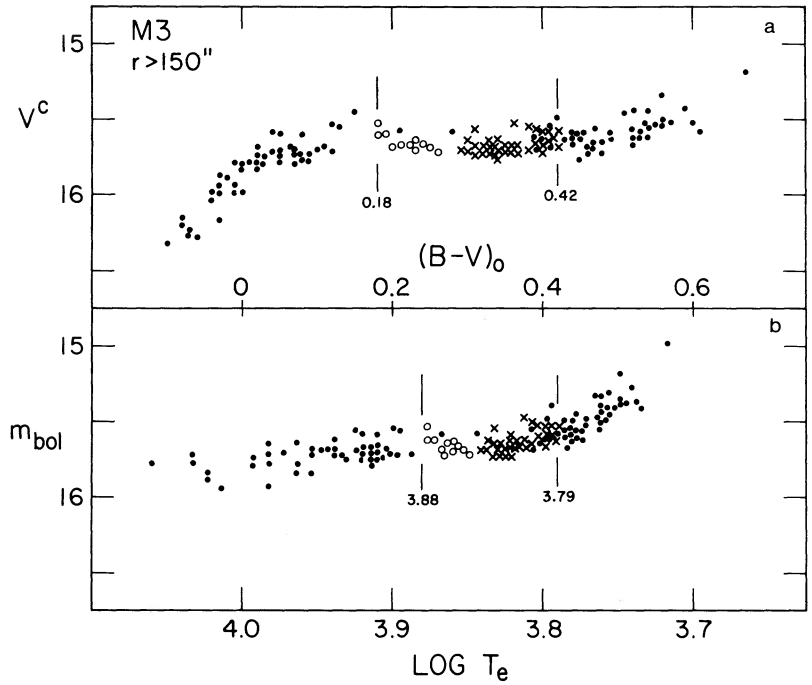

FIG. 6.—Horizontal branch for M3 from data in Tables 1 and 5. (*a*) Same as Fig. 1*a*. (*b*) The data are shown transformed into bolometric apparent magnitudes and temperatures. The RR Lyrae stars are shown as open circles for the *c* type and crosses for the *ab* type.

the test for true intrinsic scatter, consider the positions of the lines of constant period in that part of the H-R diagram that includes the variable star instability strip (cf. Sandage 1958, Fig. 3; SKS, Fig. 13). It is clear from those diagrams that the manner in which the lines of constant period cut across the ZAHB determines the shape and the slope of the ZAHB period-temperature relation. The shortest period at a given temperature is taken to define the level of the ZAHB at that temperature in the period-temperature plane. (Note, however, that in the model of LDZ this assumption is not valid for the lowest metallicity clusters because there would be no ZAHB variables in these clusters in this model). The equation of the

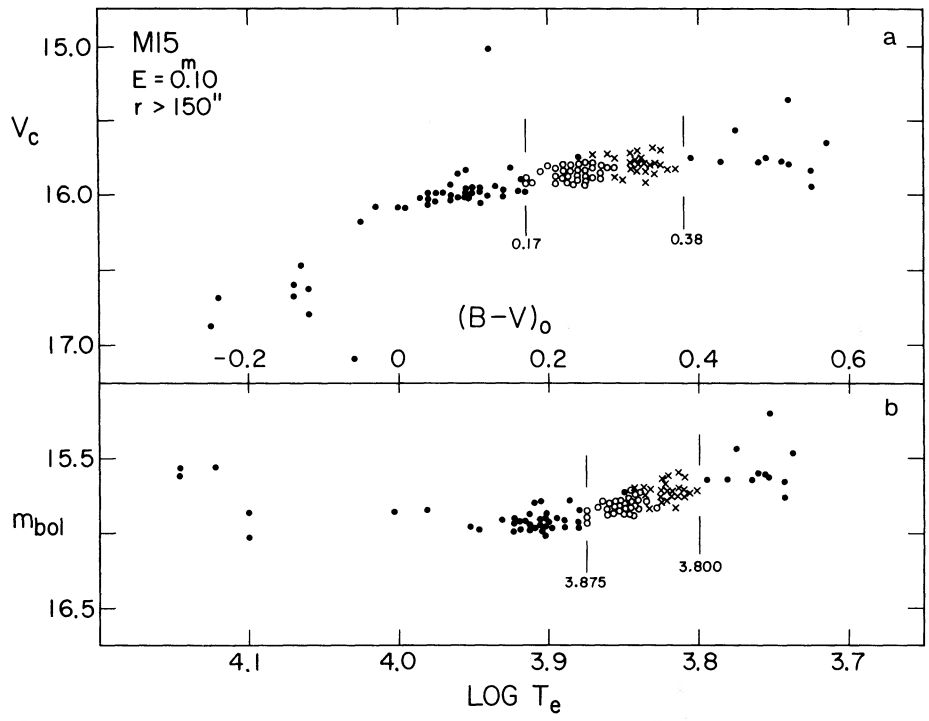

FIG. 7.—Horizontal branch for M15 from data in Tables 2 and 6, plotted (*a*) as a color-magnitude diagram and (*b*) as the H-R diagram

TABLE 6

DATA FOR RR LYRAE STARS IN M15

Star (1)	log P (2)	A_B (3)	<V> (4)	<B>-<V> (5)	$(B-V)_{st}$ (6)	$(B-V)_{st}$ (7)	m_{bol} (8)	log T_e(st)[a] (9)	log L/M (10)	Δ log P(A)[b] (11)	Δlog (T_e)[c] (12)	ΔV[d] (13)
2	-0.165	0.76	15.67	0.44	0.44	0.34	15.59	3.814	1.918	+0.068	+0.124	0.18
3	-0.410	0.61	15.83	0.34	0.34	0.24	15.80	3.850	--	--	--	0.10
4	-0.504	0.76	15.88	0.27	0.27	0.17	15.85	3.875	--	--	--	0.10
5	-0.415	0.60	15.80	0.32	0.32	0.22	15.78	3.857	--	--	--	0.14
6	-0.177	1.12	15.78	0.39	0.41	0.31	15.71	3.825	1.949	+0.102	+0.153	0.11
7	-0.435	0.69	15.87	0.31	0.31	0.21	15.85	3.861	--	--	--	0.08
8	-0.190	1.09	15.79	0.41	0.43	0.33	15.71	3.818	1.904	+0.086	+0.114	0.08
9	-0.146	0.90	15.71	0.40	0.41	0.31	15.64	3.825	1.986	+0.105	+0.184	0.17
10	-0.413	0.58	15.87	0.35	0.35	0.25	15.83	3.847	--	--	--	0.05
11	-0.464	0.72	15.85	0.29	0.29	0.19	15.83	3.868	--	--	--	0.12
12	-0.227	1.08	15.82	0.39	0.41	0.31	15.75	3.825	1.889	+0.047	+0.103	0.07
13	-0.240	1.20	15.84	0.39	0.42	0.32	15.77	3.822	1.861	+0.050	+0.078	0.05
14	-0.418	0.63	15.90	0.34	0.34	0.24	15.87	3.850	--	--	--	0.03
15	-0.234	1.05	15.89	0.37	0.39	0.29	15.84	3.833	1.914	+0.036	+0.125	0.02
16	-0.399	0.56	15.78	0.36	0.36	0.26	15.74	3.844	--	--	--	0.13
17	-0.368	0.43	15.84	0.38	0.38	0.28	15.79	3.836	--	--	--	0.06
18	-0.434	0.70	15.84	0.32	0.32	0.22	15.82	3.857	--	--	--	0.10
19	-0.242	1.54	15.81	0.32	0.38	0.28	15.76	3.836	1.917	+0.092	+0.128	0.14
20	-0.157	0.95	15.80	0.44	0.45	0.35	15.72	3.810	1.910	+0.101	+0.117	0.04
21	-0.188	1.04	15.70	0.43	0.45	0.35	15.62	3.810	1.874	+0.081	+0.086	0.16
22	-0.143	1.19	15.70	0.39	0.42	0.32	15.63	3.822	1.977	+0.146	+0.175	0.19
23	-0.199	0.98	15.80	0.41	0.42	0.32	15.73	3.822	1.910	+0.062	+0.119	0.07
24	-0.432	0.62	15.85	0.33	0.33	0.23	15.82	3.854	--	--	--	0.09
25	-0.177	1.00	15.83	0.43	0.45	0.35	15.75	3.810	1.887	+0.087	+0.097	0.03
26	-0.395	0.48	15.88	0.37	0.37	0.27	15.84	3.840	--	--	--	0.02
28	-0.174	0.93	15.82	0.42	0.43	0.33	15.75	3.818	--	--	--	0.04
29	-0.240	1.08	15.90	0.38	0.40	0.30	15.84	3.829	1.890	+0.034	+0.104	0.00
30	-0.391	0.40	15.80	0.33	0.33	0.23	15.77	3.854	--	--	--	0.14
31	-0.389	0.46	15.86	0.37	0.37	0.27	15.82	3.840	--	--	--	0.04
32	-0.218	1.22	15.72	0.35	0.38	0.28	15.67	3.836	1.946	+0.074	+0.152	0.20
35	-0.416	0.60	15.88	0.35	0.35	0.25	15.85	3.847	--	--	--	0.04
36	-0.205	1.02	15.81	0.40	0.42	0.32	15.74	3.822	1.903	+0.062	+0.113	0.07
38	-0.426	0.65	15.84	0.33	0.33	0.23	15.82	3.854	--	--	--	0.10
39	-0.409	0.52	15.85	0.35	0.35	0.25	15.82	3.847	--	--	--	0.07
40	-0.423	0.67	15.85	0.32	0.32	0.22	15.83	3.857	--	--	--	0.09
41	-0.407	0.55	15.77	0.36	0.36	0.26	15.73	3.844	--	--	--	0.14
42	-0.443	0.72	15.90	0.31	0.31	0.21	15.88	3.861	--	--	--	0.05
43	-0.402	0.64	15.86	0.32	0.32	0.22	15.84	3.857	--	--	--	0.08
44	-0.225	0.98	15.75	0.38	0.39	0.29	15.70	3.833	1.925	+0.036	+0.134	0.15
46	-0.160	1.20	15.76	0.39	0.42	0.32	15.69	3.822	1.957	+0.130	+0.158	0.13
48	-0.438	0.72	15.80	0.30	0.30	0.20	15.78	3.865	--	--	--	0.16
50	-0.526	0.67	15.92	0.27	0.27	0.17	15.89	3.875	--	--	--	0.06
51	-0.401	0.52	15.85	0.34	0.34	0.24	15.82	3.850	--	--	--	0.08
52	-0.240	1.25	15.92	0.40	0.43	0.33	15.84	3.818	1.845	+0.056	+0.064	-0.04
53	-0.383	0.52	15.80	0.34	0.34	0.24	15.77	3.850	--	--	--	0.13
54	-0.398	0.54	15.82	0.34	0.34	0.24	15.79	3.850	--	--	--	0.11
55	-0.126	0.62	15.83	0.47	0.47	0.37	15.73	3.802	1.914	+0.089	+0.118	0.00
56	-0.244	0.90	15.74	0.35	0.36	0.26	15.70	3.844	1.948	+0.007	+0.156	0.18
57	-0.457	0.57	15.76	0.34	0.34	0.24	15.73	3.850	--	--	--	0.17
58	-0.390	0.60	15.89	0.36	0.36	0.26	15.85	3.844	--	--	--	0.02
61	-0.398	0.65	15.82	0.37	0.37	0.27	15.78	3.840	--	--	--	0.08
62	-0.423	0.66	15.76	0.36	0.36	0.26	15.72	3.844	--	--	--	0.15
64	-0.439	0.74	15.86	0.32	0.32	0.22	15.84	3.857	--	--	--	0.08
65	-0.144	0.60	15.78	0.44	0.44	0.34	15.70	3.814	1.943	+0.068	+0.145	0.07
66	-0.421	0.56	15.86	0.34	0.34	0.24	15.83	3.850	--	--	--	0.07

TABLE 6—*Continued*

Star (1)	log P (2)	A_B (3)	<V> (4)	<B>-<V> (5)	$(B-V)_{st}$ (6)	$(B-V)_{st}$ (7)	m_{bol} (8)	log T_e(st)[a] (9)	log L/M (10)	Δ log P(A)[b] (11)	Δ log (T_e)[c] (12)	ΔV[d] (13)
67	-0.393	0.40	15.93	0.35	0.35	0.25	15.89	3.847	--	--	--	-0.01
74	-0.529	0.74	15.94	0.27	0.27	0.17	15.91	3.875	--	--	--	0.04
96	-0.402	0.62	15.91	0.35	0.35	0.25	15.88	3.847	--	--	--	0.01
97	-0.157	0.80	15.81	0.44	0.44	0.34	15.73	3.814	1.927	--	+0.132	0.04
101	-0.398	0.70	15.84	0.34	0.34	0.24	15.81	3.850	--	--	--	0.09
102	-0.119	0.40	15.82	0.46	0.46	0.36	15.73	3.806	1.939	--	+0.140	0.01
103	-0.434	0.73	15.87	0.33	0.33	0.23	15.85	3.854	--	--	--	0.07

[a] The temperatures in col. (9) are from the [Fe/H] = −2.0 color-temperature relation.
[b] Δ log $P(A_B)$ in col. (11) is from the M3 ZAHB lower envelope of log $P = -0.129\,A_B - 0.135$.
[c] Δ log $P(T_e)$ in col. (12) is from the M3 ZAHB lower envelope of log $P = -3.70$ log $T_e = 13.823$.
[d] ΔV in col. (13) is relative to the *C-M* diagram lower envelope of $V = 16.20 - 0.8\,(B-V)$.

fiducial line in Figure 4*b* is

$$\log P = -3.70 \log T_e + 13.823 . \quad (1)$$

We adopt this equation as the reference period-temperature line from which to measure the "period shift at constant T_e" for each cluster discussed in this section. The difference between the observed log P and that calculated from this equation is *defined* as the period shift.[1] Note that, although this envelope line is *close* to the position of the ZAHB, it must be slightly too cool because of errors in log T_e due to measuring errors in $B-V$ that translate to $\sigma(\Delta \log T_e) \sim 0.006$. However, this small difference between the true ZAHB line and the adopted envelope line in Figure 4*b* is irrelevant for the purposes of this paper, since we deal here only with *changes* in the Δ log P period shifts as a function of observed magnitude.

Consider first the data for M3 in Table 5. The "static star" color defined in § IV as $\langle B\rangle - \langle V\rangle + \Delta C(A)$ is listed in column (6) and labeled $(B-V)_{st}$; the resulting log T_e in column (8) is obtained from the calibrations in § III; the Δ log $P(A_B)$ period shifts at constant amplitude in column (10) are calculated so as to address the problem of differential reddening using the envelope of the *period-amplitude relation for M3* as explained and used in Appendix A; the Δ log $P(T_e)$ period shifts at constant temperature in column (11) are calculated from the lower envelope of the M3 *period-temperature* relation. The difference between the observed apparent V-magnitude and that of the ZAHB at the observed color of the star, as read from Figure 1*a*, is given in column (12). The sense of the difference is that a positive ΔV value signifies a brighter *observed* magnitude than that which would obtain (at a given color) on the ZAHB.

The luminosity-to-mass ratio in column (9) of Table 5 is calculated from the pulsation equation

$$\log (L/M^{0.81}) = (\log P + 3.48 \log T_e - 11.497)/0.84 , \quad (2)$$

which follows from the calculation of van Albada and Baker (1971). This is closely the same equation as that obtained by Iben (1971) and by Cox (1987).

Figure 9 shows the correlation between observed magnitude of an individual RR Lyrae star in M3 and the difference between the observed period and the period on the envelope line of Figure 4*b* at the observed temperature. Shown in Figure 9*a* is the H-R diagram for the RR*ab* Lyrae stars alone, illustrating the spread of about 0.2 mag discussed in previous sections. [The $T(1)$ temperature scale of S81*b* is used; otherwise Figure 9*a* is an enlargement of the RR Lyrae region of Figs. 6 and 8.] Figure 9*b* shows the correlation of the observed V-magnitude with the log of this period ratio (i.e., the period shift) at constant temperature, using the data from Table 5. (Because the lower envelope of the HB at $V = 15.74$ is *level* in M3, the use of V_c values as the ordinate in Figure 9*b* is equivalent to using the ΔV magnitude difference in col. [12] for this cluster.)

The correlation between observed magnitude and period shift is evident, showing that the observed magnitude spread in Figure 9*a* is real. The slope of the least-squares line found by *averaging*[2] the two solutions made by interchanging the independent variables is $dV/d\,\Delta \log P(T_e) = -1.77$, as shown in Figure 9*b*. The theoretical slope, obtained from equation (1) if we were to assume constant mass for all stars in Figure 9, is $d \log L = 1.19\, d \log P$ at constant T_e, or d mag $= 2.98\, d \log P$. A slope of 3 was used for this relation in the previous discussions (SKS; S81*b*, S82).

The necessary data for M15 are listed in Table 6. The magnitude difference in column (13) is between the observed luminosity and the luminosity of the *sloping* ZAHB at a given color (cf. Figs. 1*b*, 7, and 8*b*) whose equation is at the foot of Table 6.

[1] For this paper these shifts are, then, taken to be relative to the envelope line in Fig. 4*b of M3*. It is important to note that the *smallest* period shifts in any given cluster determine the period shift *of that cluster's ZAHB* relative to M3. But note also that the period-shift phenomenon discussed in the *present paper* is not the period shift of the *ZAHB* as [Fe/H] is changed from one cluster to another, as will be discussed in the paper that follows (Sandage 1990), but is the period shift of *each* variable *in a given cluster* relative to the M3 fiducial line in Fig. 4*b*. These period shifts due to luminosity evolution brightward from each cluster's ZAHB do not constitute the Oosterhoff period dichotomy effect, which, rather, is the separation of individual clusters into two period groups when a mean period is used as an ensemble average of all variables in that cluster: cf. Sandage (1990).

[2] According to Seares (1944), the theoretically correct procedure to find the impartial slope of a linear regression where the errors in the ordinate and abscissa values are equal is not to average the two solutions but to take the square root of the product of the two slopes determined by interchanging dependent and independent variables in the resulting two least-squares solutions. In the present case, this gives an impartial slope of −1.51 rather than −1.77 for the M3 Δ log $P(T_e)$, ΔV correlation. For the present purposes, the difference in these two values of the slope is unimportant. In any case, the exact ratio of errors between ordinate and abscissa is unknown, which is also the general case in practice in most similar problems, often making the exact procedure largely academic. That there are errors in both ordinate *and* abscissa of Fig. 9 is evident; besides the measuring error of $\sigma(V) \sim 0.015$ mag in V, an error in Δ log P exists because of an error in the measured log T_e based on $\sigma(B-V) \sim 0.020$ mag. This error translates to $\sigma(\log T_e) \sim 0.007$, which, via eq. (1), gives $\sigma(\Delta \log P) \sim 0.026$, similar to the estimated $\sigma(\Delta V) \sim 0.015$ mag for the ordinate.

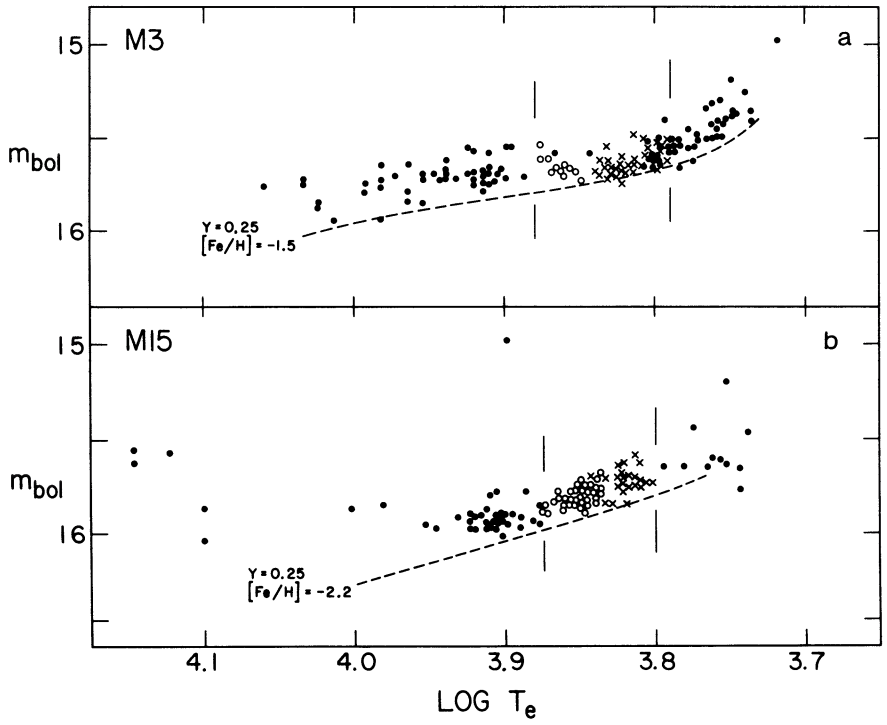

FIG. 8.—Comparison of the H-R diagrams of M3 and M15 with the theoretical ZAHB models of Sweigart and Gross (1976) for (*a*) [Fe/H] = −1.5 and (*b*) [Fe/H] = −2.2, both with $Y = 0.25$.

The H-R diagram in Figure 10*a* uses the $\langle B \rangle - \langle V \rangle$ colors given by Bingham *et al.* (1984). The M15 period shifts relative to the M3 ZAHB period-temperature relation, listed in column (12), are plotted against the magnitude deviations ΔV in Figure 10*b*. The slope of the correlation is $d\,\Delta V = 2.69d\,\Delta \log P(T_e)$ with a correlation coefficient of $r = 0.60$.[3] Because a correlation exists in a similar fashion to that for M3, we conclude again that the observed spread of the M15 RR Lyrae magnitudes is real; the brightest variables at a given temperature have longer periods. The total intrinsic width of the M15 HB at the RR Lyrae strip is 0.2 mag, found from the $\Delta \log P$ values, closely the same as the separation of the envelope lines in Figure 1*b*.

Data for the variables in NGC 6981 analyzed by Dickens and Flinn (1972) are given in Table 7. Distance-to-center crowding corrections, determined from the HB stars in NGC 6981 that were measured by Dickens (1972), have been applied to the V-magnitudes listed by Dickens and Flinn to obtain the values in column (4). (These corrections, used earlier in S81*b*

[3] As with the M3 data above, and also as with the other clusters discussed below, the slope of 2.7 is smaller than the "constant mass" slope of 3.0 obtained from eq. (2) at constant T_e. However, none of these slope determinations are robust enough to establish a mass difference between evolved RR Lyrae stars and those on the ZAHB of a given cluster. Nevertheless, if the slopes in Figs. 9*b* and 10*b* and in other similar diagrams were, in fact, *less* than 3.0, then the masses of the evolved (bright) variables would be *smaller* than those on the ZAHB at the same temperature. In that case, the brighter (i.e., evolved) RR Lyrae variables would have to have come from the lower mass ZAHB stars blueward of the RR Lyrae instability strip. Hence, the direction of the post–ZAHB evolution tracks in these clusters could be established as being toward brighter magnitudes and *cooler* temperatures as they cross the RR Lyrae strip on their way to the asymptotic giant branch. More precise photometry should permit this mass test via correlations such as those in panels *b* in Figs. 9–13 to be reliable.

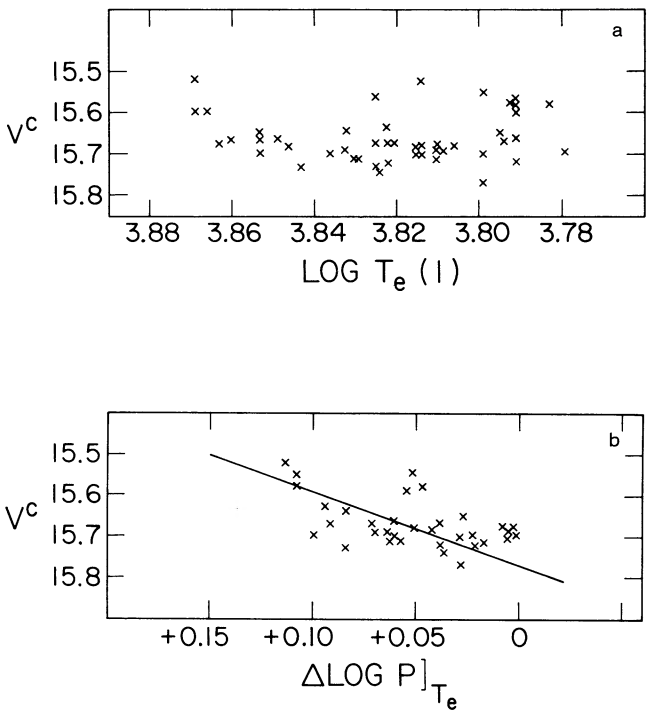

FIG. 9.—(*a*) H-R diagram for the M3 RR*ab* Lyrae stars, showing the observed spread of $\Delta V \approx 0.2$ mag. The temperature scale is $T(1)$ from Sandage (1981*b*). These $T(1)$ temperatures are very nearly the same as those obtained from $\langle B \rangle - \langle V \rangle + C(A)$. (*b*) Correlation of the observed magnitude with the deviation from the period-temperature lower envelope line at fixed temperature. The sense of the correlation is that brighter stars have longer periods relative to the expected periods on the ZAHB at the same temperature. The data are from Table 5.

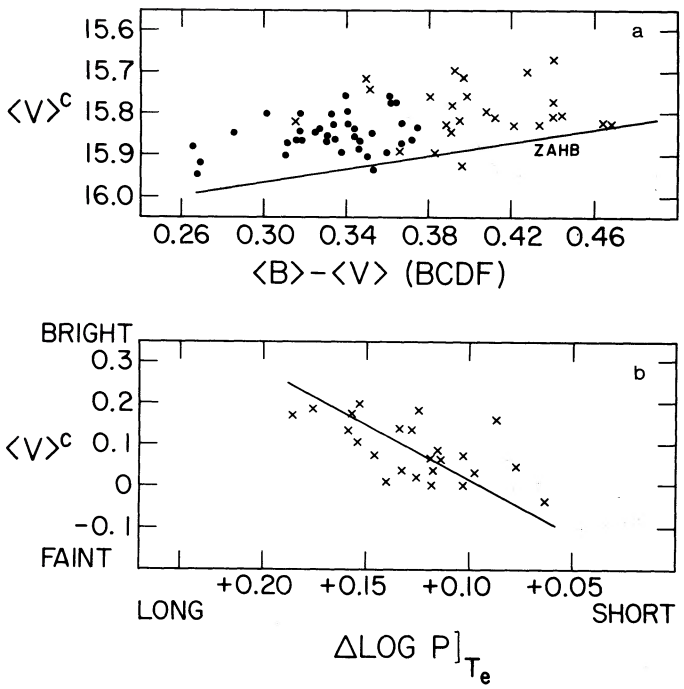

FIG. 10.—Same as Fig. 9, but for M15. The data are from Table 6.

[Table 5], were not tabulated; they are 0.24 mag at $r = 40''$, 0.17 mag at $r = 60''$, 0.11 mag at $r = 80''$, 0.05 mag at $r = 120''$, and 0.00 mag beyond $r = 200''$.) The "static star" color in column (6) is corrected for the adopted reddening of $E(B-V) = 0.04$ to give the corrected color in column (7), transformed to log T_e in column (8) using the relation in § III for [Fe/H] = −1.5. Columns (9), (10), and (11) are similar to the equivalent columns in Tables 5 and 6.

The color-magnitude diagram for the RR Lyrae stars from these data and for the nonvariable HB stars measured by Dickens (1972), corrected for distance to center, is shown in Figure 11*a*. Envelope lines are drawn by eye similar to those in Figure 1. The HB of NGC 6981 is evidently somewhat wider than the branches in M3 and M15. The brightest variable is V27. It has the longest period relative to others of its temperature, but membership in NGC 6981 is in some doubt. The distance from the cluster center at 314″ is larger than for any other variable listed by Sawyer Hogg (1973). Nevertheless, the star fits the expectations of the period-shift–magnitude relation in Figure 11*b* put through the fainter variables. The slope of the impartial least-squares correlation is $dV/d\,\Delta \log P(T_e) = -1.69$ with a correlation coefficient of 0.84, weighted heavily, of course, by the data for V27 itself.

Data for the variables in NGC 6171, shown in Figure 12*a*, are shown in Table 8, based on the measurements of Dickens (1971). Data for the nonvariable stars, not listed, are from Dickens and Rolland (1972). The adopted reddening of $E(B-V) = 0.32$ is used to convert the observed colors of the variables (corrected by Fig. 5) to the reddening-free "static star" colors in column (5). The temperatures in column (6) are based on these colors and on the color-temperature calibration of § III for [Fe/H] = −1.0. The magnitudes have been corrected for distance-to-center contamination by amounts which can be found by comparing the values in column (4) of Table 8 with those in Table 6 of Dickens (1971). No contamination corrections were needed for the nonvariable HB stars. The impartial least-squares line shown in Figure 12*b* has a slope of 2.55 with a correlation coefficient $r = 0.73$. The total width of the HB in NGC 6171 is ~0.5 mag.

The final cluster for which we illustrate the data is NGC 6121 (M4), shown in Figure 13 using photoelectric data by Sturch (1977) and Cacciari (1979) for the variables, and the photographic photometry by Lee (1977*a*) for the nonvariable

TABLE 7

PHOTOMETRIC PARAMETERS FOR RR LYRAE STARS IN NGC 6981

Star (1)	Log P (2)	A_B (3)	<V>^{c} (4)	[<B>-<V>]^c (5)	(B-V)$^c_{st}$ (6)	(B-V)$^{o,c}_{s,t}$ (7)	log $T_e{}^a_{,st}$ (8)	log $L/M^{0.81}$ (9)	Δ log P(A)^b (10)	Δlog P(T_e)^c (11)
					E=0.04					
2	-0.332	1.66	16.99	0.26	0.33	0.29	3.839	1.822	0.017	0.049
3	-0.303	1.58	16.93	0.29	0.35	0.31	3.832	1.828	0.036	0.052
4	-0.258	1.18	16.95	0.39	0.42	0.38	3.806	1.774	0.029	0.001
7	-0.280	1.17	16.99	0.37	0.40	0.36	3.814	1.781	0.006	0.009
8	-0.245	1.01	17.05	0.40	0.42	0.38	3.806	1.789	0.020	0.014
9	-0.220	0.80	17.05	0.45	0.45	0.41	3.795	1.773	0.018	-0.002
10	-0.253	1.08	17.00	0.40	0.42	0.38	3.806	1.780	0.021	0.006
11	-0.284	0.91	17.08	0.43	0.44	0.40	3.799	1.714	-0.032	-0.051
15	-0.259	0.93	16.99	0.41	0.42	0.38	3.806	1.772	-0.004	0.000
17	-0.241	1.05	17.05	0.40	0.42	0.38	3.806	1.794	0.029	0.018
21	-0.275	1.29	17.06	0.41	0.45	0.41	3.795	1.708	0.026	-0.057
23	-0.233	0.78	17.00	0.47	0.47	0.43	3.787	1.725	0.003	-0.044
25	-0.452	0.56	16.92	0.28	0.28	0.24	3.856	--	--	--
27	-0.171	1.49	16.74	0.32	0.38	0.34	3.822	1.944	0.156	0.147
28	-0.246	0.81	16.97	0.41	0.41	0.37	3.810	1.805	-0.007	0.028
29	-0.218	0.80	16.94	0.43	0.43	0.39	3.803	1.809	0.020	0.030
32	-0.277	0.94	17.01	0.39	0.40	0.36	3.814	1.784	-0.021	0.012
35	-0.265	0.97	17.01	0.39	0.40	0.36	3.814	1.798	-0.005	0.024

NOTE.—From data of Dickens and Flinn 1972.

[a] Temperatures in col. (8) are from the [Fe/H] = −1.5 color-temperature relation.

[b] Δ log $P(A_B)$ in col. (10) is relative to M3 ZAHB lower envelope of log $P = -0.129A_B - 0.135$.

[c] Δ log $P(T_e)$ in col. (11) is relative to M3 ZAHB lower envelope of log $P = -3.70$ log $T_e + 13.823$.

TABLE 8

PHOTOMETRIC PARAMETERS FOR RR LYRAE STARS IN NGC 6171

Star (1)	log P (2)	A_B (3)	<V>[c] (4)	E=0.32 $(B-V)^0_{st}$ (5)	log T_e[a] (6)	log L/M[a,8] (7)	Δlog P(A)[b] (8)	Δlog P(T_e)[c] (9)
1	-0.490	0.57	15.62	0.25	3.857	--	--	--
2	-0.243	1.03	15.64	0.40	3.806	1.792	0.025	0.016
3	-0.247	0.69	15.43	0.37	3.816	1.828	-0.023	0.049
4	-0.550	0.66	15.55	0.16	3.886	--	--	--
5	-0.153	0.57	15.52	0.44	3.792	1.841	0.056	0.054
6	-0.585	0.65	15.58	0.19	3.876	--	--	--
7	-0.301	1.04	15.65	0.42	3.799	1.693	-0.032	-0.068
8	-0.252	1.35	15.57	0.41	3.803	1.768	0.057	-0.004
9	-0.494	0.62	15.63	0.31	3.837	--	--	--
10	-0.381	1.40	15.79	0.34	3.827	1.714	-0.065	-0.044
11	-0.227	0.81	15.71	0.47	3.782	1.711	0.012	-0.057
12	-0.325	1.31	15.69	0.36	3.820	1.752	-0.021	-0.014
13	-0.331	1.63	15.81	0.38	3.813	1.716	0.014	-0.046
14	-0.317	1.73	15.66	0.38	3.813	1.732	0.041	-0.032
15	-0.540	0.59	15.62	0.20	3.873	--	--	--
16	-0.282	1.05	15.68	0.43	3.795	1.700	-0.012	-0.064
17	-0.251	1.34	15.56	0.36	3.820	1.840	0.057	0.097
18	-0.248	1.12	15.74	0.41	3.803	1.773	0.031	0.041
19	-0.555	0.66	15.75	0.23	3.863	--	--	--
20	-0.238	0.92	15.60	0.44	3.792	1.739	0.016	0.018

NOTE.—From data of Dickens 1971.

[a] Temperatures in col. (6) are from the [Fe/H] = −1.0 color-temperature relation.

[b] Δ log $P(A)$ in col. (8) is from the M3 ZAHB lower envelope relation of log $P = -0.129A_B - 0.135$.

[c] Δ log $P(T_e)$ in col. (9) is from the M3 ZAHB lower envelope relation of log $P = -3.70$ log $T_e + 13.823$.

HB stars. The mean B and V magnitudes for the variables, read from the photoelectric light curves, are listed in columns (4) and (5) of Table 9. The resulting $\langle B\rangle - \langle V\rangle$ values are converted to "static star" colors in column (6) using Figure 5. The adopted reddenings for *individual* stars determined by Cacciari (1979), accounting therefore for differential reddening, are in column (8), which, when applied to column (7), gives column (9). The temperatures in column (10) are based on column (9) and on the calibration in § III for [Fe/H] = −1.0. Columns (11), (12), and (13) are again self-explanatory. The period-shift–magnitude relation in the bottom panel of Figure 13, plotted from data in columns (4) and (13) of Table 9, has a slope of 2.33 (note again that it is smaller than 3.0) with a correlation coefficient of $r = 0.93$).

The total width of the HB from the RR Lyrae stars alone, found from the range of the ordinate in Figure 13*b*, is 0.55 mag. This is close to the value found from Figure 13*a* using the nonvariable stars. A confirmation of the large width is available from the independent photometry of the HB in M4 by Alcaino and Liller (1984), seen from the *C-M* diagram in their Figure 6. Note that their subgiant branch, and also that of Lee (1977*b*), is very narrow in $B-V$, showing that any differential reddening is smaller than $\Delta E(B-V) \sim 0.02$ mag over the region of the cluster measured in each study.[4]

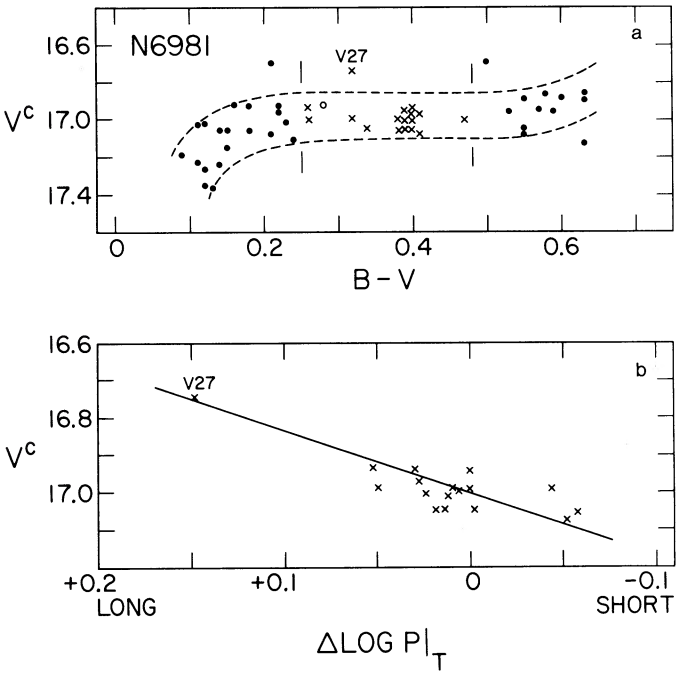

FIG. 11.—Same as Figs. 9 and 10, but for NGC 6981 from data in Table 7. Nonvariable HB stars are plotted in (*a*) from data of Dickens (1972, Table II).

[4] This point concerning differential reddening is important because the vector of such reddening in Fig. 13*b* (and in the corresponding diagrams of the other clusters as well) is very nearly *along the correlation line.* This is seen by considering two stars differentially reddened by $\Delta E(B-V)$. The more obscured star will be fainter by $\Delta V \sim 3\Delta E(B-V)$ and will appear cooler by Δ log $T_e \sim 0.33\Delta E(B-V)$. This will cause a spuriously short period shift to be calculated whose error is Δ log $P \sim 3.7\ \Delta$ log $T \sim 1.2\Delta E(B-V)$ according to eq. (1). Hence, the differential reddening vector has a slope of $d\ \Delta V \sim 2.5\ \Delta$ log P, *which is close to the slopes of the observed correlations.* Note, however, that if the entire effect in Fig. 13*b* were to be ascribed to differential reddening, the size of the effect (i.e., the range of ~0.6 mag in ΔV, or 0.25 in Δ log P) requires $\Delta E(B-V)$ to be 0.2 mag for the differential reddening across M4. Such a large value is not supported by the *C-M* diagram of the subgiant branch or by the individual photoelectric photometry of the variables themselves (Sturch 1977; Cacciari 1979). Nevertheless, the reality of the correlations similar to that in Fig. 13*b* for the other clusters is so central to the conclusions of this paper that we consider in Appendix A the equivalent formulation of the period shift at *constant amplitude* for many of the clusters discussed here. The formulation using constant amplitude is, of course, independent of temperature, and therefore of reddening. Anticipating the conclusion of the discussion in Appendix A, the similarity of the period shifts at constant temperature and at constant amplitude shows that differential reddening is not a significant effect in the observed correlations in any of the clusters.

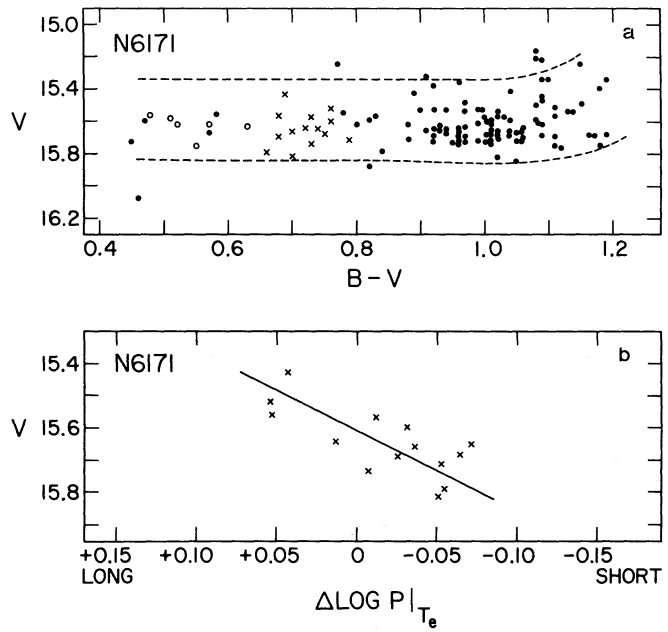

FIG. 12.—Same as Figs. 9–11, but for NGC 6171 from data in Table 8. Nonvariable HB stars are from Dickens and Rolland (1972, Table II).

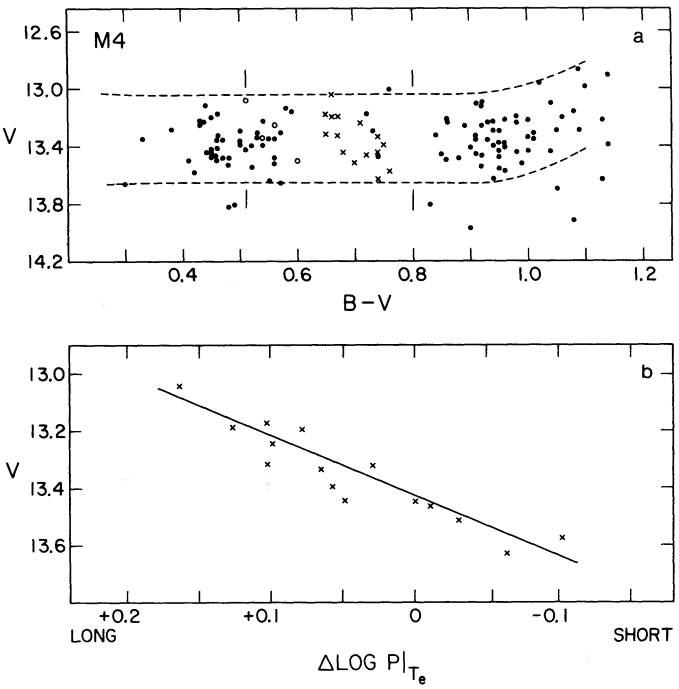

FIG. 13.—Same as Figs. 9–12, but for M4 from data in Table 9. Data for the nonvariable HB stars are from Lee (1977*a*).

To increase the sample size, color data for RR Lyrae variables in three more clusters where the photometric accuracy is adequate are set out in Tables 10, 11, and 12. These data are not illustrated but are given here for their use in the next section and the paper that follows (Sandage 1990).

Data for the variables in NGC 6723 measured by Menzies (1974) are given in Table 10. Stars marked with an asterisk have uncertain photometry according to Menzies, because of crowding. Corrections for crowding, listed in column (6), have been made by correlating the measured magnitudes of the HB stars listed by Menzies with distance to center. The corrected magnitudes are given in column (7). The other columns are

TABLE 9

PHOTOMETRIC PARAMETERS FOR RR LYRAE STARS IN M4

Star (1)	log P (2)	A_B (3)	<V> (4)	<B> (5)	<B>-<V> (6)	$(B-V)_{st}$ (7)	E (8)	$(B-V)^o_{st}$ (9)	log T_e(st)[a] (10)	logL/$M^{0.81}$ (11)	Δ log P(A)[b] (12)	Δlog P(T_e)[c] (13)
2	-0.271	1.37	13.44	14.14	0.70	0.74	0.37	0.39	3.809	1.771	0.041	0.001
5	-0.206	0.43	13.33	14.07	0.74	0.74	0.35	0.39	3.809	1.848	-0.016	0.064
6	-0.494	0.61	13.49	14.09	0.60	0.60	--	0.25	3.857	--	--	--
7	-0.302	1.22	13.44	14.09	0.65	0.68	0.39	0.33	3.830	1.821	-0.010	0.046
11	-0.307	1.02	13.46	14.16	0.70	0.72	0.33	0.37	3.816	1.757	-0.040	-0.011
12	-0.351	1.55	13.57	14.27	0.70	0.76	0.36	0.41	3.803	1.651	-0.016	-0.103
14	-0.334	1.58	13.63	14.31	0.68	0.74	0.43	0.39	3.809	1.696	0.005	-0.064
15	-0.353	1.54	13.51	14.15	0.64	0.70	0.37	0.35	3.823	1.731	-0.019	-0.031
19	-0.330	1.48	13.32	13.94	0.62	0.67	0.35	0.32	3.833	1.800	-0.004	0.029
27	-0.213	1.22	13.24	13.92	0.68	0.71	0.34	0.36	3.820	1.885	0.079	0.098
28	-0.282	1.24	13.17	13.79	0.62	0.65	0.30	0.30	3.840	1.886	0.013	0.103
29	-0.282	1.24	13.31	13.93	0.62	0.65	0.33	0.30	3.840	1.886	0.013	0.103
30	-0.569	0.75	13.34	13.87	0.53	0.53	--	0.18	3.880	--	--	--
31	-0.296	1.38	13.19	13.81	0.62	0.66	0.24	0.31	3.837	1.857	0.017	0.078
32	-0.237	1.02	13.18	13.82	0.64	0.66	0.32	0.31	3.837	1.927	0.030	0.126
33	-0.211	1.21	13.04	13.67	0.63	0.66	0.30	0.31	3.837	1.958	0.080	0.163
35	-0.203	0.78	13.39	14.14	0.75	0.75	0.42	0.40	3.806	1.839	0.033	0.056
42	-0.518	0.53	13.25	13.81	0.56	0.56	--	0.21	3.870	--	--	--
43	-0.494	0.59	13.08	13.59	0.51	0.51	--	0.16	3.886	--	--	--

$\overline{<E>} = 0.35$

NOTE.—From photoelectric data of Sturch 1977 and Cacciari 1979.

[a] Temperatures in col. (10) are from the [Fe/H] = −1.0 color-temperature relation.

[b] Δ log $P(A)$ in col. (12) is from the M3 ZAHB lower envelope relation of log $P = -0.129A_B - 0.135$.

[c] Δ log $P(T_e)$ in col. (13) is from the M3 ZAHB lower envelope relation of log $P = -3.70$ log $T_e + 13.823$.

TABLE 10

PHOTOMETRIC PARAMETERS FOR RR LYRAE STARS IN NGC 6723

Star (1)	r" (2)	log P (3)	A_B (4)	<V> (5)	V(Cr) (6)	<V>[c] (7)	<B>-<V> (8)	C(A) (9)	$(B-V)_{st}$ (10)	log T_e[a] (11)	log $L/M^{0.81}$ (12)	Δ log P(A)[b] (13)	Δlog $P(T_e)$[c] (14)
1	213	-0.269	0.48	15.62	0.00	15.62	0.39	0.00	0.39	3.809	1.773	-0.072	+0.001
2	157	-0.298	1.74	15.27	0.00	15.27	0.32	0.07	0.39	3.809	1.738	+0.061	-0.028
3	244	-0.306	1.77	15.38	0.00	15.38	0.30	0.08	0.38	3.813	1.746	+0.057	-0.021
7	210	-0.512	0.61	15.60	0.00	15.60	0.24	0.00	0.24	3.860	--	--	--
9*	76	-0.240	1.35	15.27	+0.33	15.60	0.32	0.04	0.36	3.820	1.853	+0.069	+0.071
10	171	-0.598	0.63	15.54	0.00	15.54	0.17	0.00	0.17	3.883	--	--	--
11	265	-0.272	1.37	15.46	0.00	15.46	0.33	0.04	0.37	3.816	1.798	+0.040	+0.024
13*	85	-0.294	1.51	15.19	+0.25	15.44	0.27	0.06	0.33	3.830	1.830	+0.036	+0.054
15	192	-0.361	1.69	15.33	0.00	15.33	0.25	0.07	0.32	3.833	1.763	-0.008	-0.002
16*	104	-0.157	1.12	15.12	+0.14	15.26	0.37	0.02	0.39	3.809	1.906	+0.122	+0.113
17	111	-0.276	1.34	15.58	+0.10	15.68	0.37	0.04	0.41	3.803	1.740	+0.032	-0.028
18	139	-0.279	1.14	15.45	+0.02	15.47	0.33	0.02	0.35	3.823	1.819	+0.003	+0.043
19	203	-0.272	1.37	15.52	0.00	15.52	0.42	0.04	0.46	3.785	1.670	+0.040	-0.091
21*	84	-0.226	1.20	15.28	+0.26	15.54	0.31	0.03	0.34	3.826	1.895	+0.064	+0.107
22*	80	-0.511	0.54	15.23	+0.29	15.52	0.31	0.00	0.31	3.837	--	--	--
24	162	-0.523	0.61	15.52	0.00	15.52	0.29	0.00	0.29	3.844	--	--	--
27	241	-0.208	0.82	15.49	0.00	15.49	0.43	0.00	0.43	3.796	1.792	+0.033	+0.014
31*	84	-0.214	0.85	15.29	+0.26	15.55	0.33	0.01	0.34	3.827	1.913	+0.031	+0.123
32*	102	-0.543	0.39	15.19	+0.15	15.34	0.14	0.00	0.14	3.890	--	--	--

NOTE.—From data of Menzies 1974. An asterisk following a star number in col. (1) means that Menzies indicates the photometry is uncertain because of crowding.

[a] Temperatures in col. (11) from [Fe/H] = −1.0 color-temperature relation with $E = 0.00$.

[b] Δ log $P(A)$ in col. (13) relative to M3 ZAHB lower envelope as $\log P = -1.29 A_B - 0.135$.

[c] Δ log $P(T_e)$ in col. (14) relative to M3 ZAHB lower envelope as $\log P = -3.70 \log T_e + 13.823$.

TABLE 11

PHOTOMETRIC PARAMETERS FOR RR LYRAE STARS IN NGC 6712

Star (1)	% (2)	log P (3)	A_B (4)	<V>[c] (5)	<B>-<V> (6)	$(B-V)_{st}$ (7)	$(B-V)^0_{st}$ E=0.42 (8)	log $T_{e,st}$[a] (9)	log $L/M^{0.81}$ (10)	Δlog P(A)[b] (11)	Δlog $P(T_e)$[c] (12)
1	97	-0.291	1.14	16.28	0.76	0.78	0.36	3.820	1.792	-0.009	0.020
3	97	-0.183	0.68	16.25	0.85	0.85	0.43	3.796	1.822	0.040	0.039
4	59	-0.213	0.66	16.53	0.86	0.86	0.44	3.792	Field	0.007	--
5	--	-0.263	1.40	16.08	0.82	0.87	0.45	3.788	1.693	0.053	-0.070
6	79	-0.292	1.52	16.25	0.84	0.90	0.48	3.779	1.621	0.039	-0.133
12	97	-0.299	1.54	16.30	0.76	0.82	0.40	3.806	1.725	0.035	-0.040
13	98	-0.250	1.38	16.16	0.65	0.69	0.27	3.850	1.965	0.063	0.172
18	93	-0.462	0.62	16.29	0.77	0.77	0.35	3.823	--	--	--
19	41	-0.373	0.42	16.05	0.80	0.80	0.38	3.813	Field	--	--
20	--	-0.480	0.54	16.40	0.68	0.68	0.26	3.854	--	--	--

NOTE.—Data from Sandage, Smith, and Norton 1966.

[a] Temperatures in col. (9) are based on the [Fe/H] = −1.0 color-temperature relation.

[b] Δ log $P(A_B)$ in col. (11) is relative to the M3 ZAHB lower envelope at log $P = -0.129A_B - 0.135$.

[c] Δ log $P(T_e)$ in col. (12) is relative to the M3 ZAHB lower envelope at log $P = -3.70 \log T_e + 13.823$.

similar to the equivalent columns in the previous tables. Note from column (14) that the four stars with the *smallest* period shifts, defining therefore the stars in this sample which are closest to the ZAHB, give a mean value of $\langle\Delta \log P(T_e)\rangle = -0.42$ for the ZAHB of NGC 6723 relative to the ZAHB of M3. The mean value of $\langle\log (L/M^{0.81})\rangle$ for these three stars in NGC 6723 is 1.724, to be used in the following paper as an approximation to the log $(L/M^{0.81})$ value of the ZAHB of this cluster.

Data for the variables in NGC 6712, measured by Sandage, Smith, and Norton (1966) and corrected to the magnitude system of Cudworth (1988), are listed in Table 11 with a format similar to that of previous tables. Listed in column (2) is the probability of cluster membership given by Cudworth from his proper-motion measurements. It is likely that V4 and V19 are not members. From the data in columns (10) and (12) for the few members we adopt $\langle\log (L/M^{0.81})\rangle = 1.680$ and the uncertain value of $\langle\Delta \log P(T_e)\rangle = -0.081$ for the ZAHB of NGC 6712, to be used in a following paper on the Oosterhoff period effect *between* clusters. These data, as before, are based on the three stars in NGC 6712 with the lowest period-shift values.

Finally, data for the few RR Lyrae stars in M92 (NGC 6341) are listed in Table 12, based on data from Arp, Baum, and Sandage (1953, Table V). Their listed colors have been transformed to the $B-V$ color system by adding 0.16 mag to their $P-V$ colors, determined by comparing the normal points of the M92 *C-M* diagram given by Sandage and Walker (1966, Table 4) in $B-V$ with the *C-M* diagram of Arp, Baum, and Sandage in their $P-V$ color system. (In Table 12 note the revised period for V8, taken here from Sawyer Hogg 1973, based on Oosterhoff 1944, rather than from Hachenberg 1939.) Again, for the purposes of a following paper, the values of the adopted M92 ZAHB period shift and luminosity-to-mass ratio are $\langle\Delta \log P(T_e)\rangle = 0.082$ and $\langle\log (L/M^{0.81})\rangle = 1.871$ obtained from the data in Table 12 for the three stars with the smallest $\Delta \log P(T_e)$ values.

VII. INTRINSIC WIDTH OF THE HORIZONTAL BRANCH AS A FUNCTION OF METALLICITY

We now approach the central problem of this investigation, which is to set out the available reliable data on HB widths in a number of clusters so as to determine the size of the intrinsic spread of RR Lyrae star absolute magnitudes at a given metallicity. The problem is important in the use of these variables as distance indicators, both in the Galaxy and for the extragalactic distance scale. In this section we increase the sample size by using clusters without two-color RR Lyrae data. To do so, we use the results of the last section which show that the

TABLE 12

PHOTOMETRIC PARAMETERS FOR RR LYRAE STARS IN M92

Star (1)	log P (2)	A_B (3)	$\langle V\rangle$ (4)	$(B-V)^0_{st}$ $(E = 0.02)$ (5)	log $T_{e,st}$[a] (6)	log $(L/M^{0.81})$ (7)	Δ log $P(A_B)$[b] (8)	Δ log $P(T_e)$[c] (9)
1.....	−0.153	0.89	15.09	0.37	3.802	1.882	0.097	0.091
2.....	−0.191	1.02	15.08	0.34	3.814	1.887	0.076	0.098
3.....	−0.196	1.12	15.29	0.28	3.836	1.972	0.083	0.174
5.....	−0.208	1.02	15.07	0.31	3.825	1.912	0.059	0.122
8.....	−0.172	1.09	15.16	0.38	3.798	1.843	0.104	0.058
10.....	−0.423	0.60	15.05	0.29	3.833	...	...	...

NOTE.—Data from Arp, Baum, and Sandage 1953, Table V.

[a] Temperatures in col. (6) are based on the [Fe/H] = −2·0 color-temperature relation.

[b] Δ log $P(A_B)$ in col. (8) is relative to the M3 ZAHB lower envelope at log $P = -0.129A_B - 0.135$.

[c] Δ log $P(T_e)$ in col. (9) is relative to the M3 ZAHB lower envelope at log $P = -3.70 \log T_e + 13.823$.

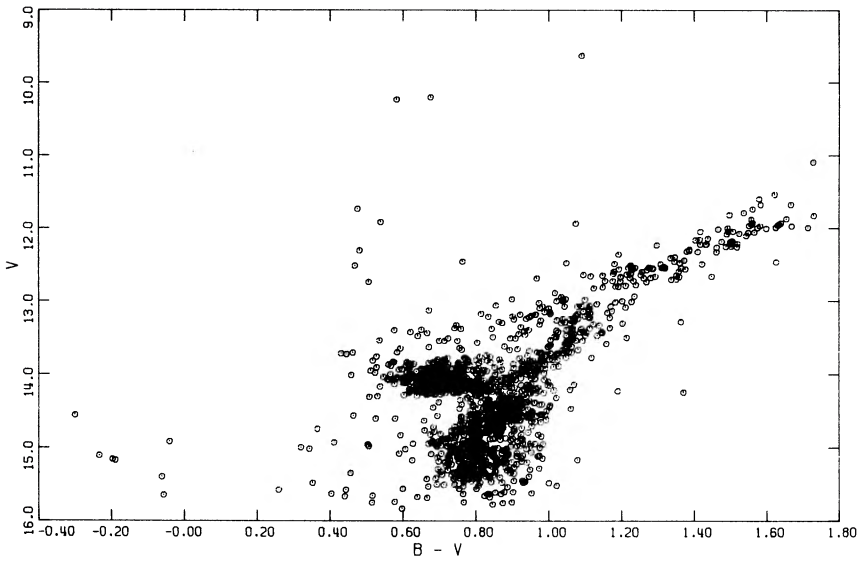

FIG. 14.—Color-magnitude diagram for 1500 stars in 47 Tuc from an unpublished study that combines measurements of four plates in each color from Siding Spring (Australia) with four plates in each color from Las Campanas (Chile), shown here to illustrate the nature of the evolution tracks away from the ZAHB on their way to the AGB.

intrinsic width of the HB that is inferred from the apparent magnitude dispersion of nonvariable HB stars blueward and redward of the RR Lyrae strip is the same as the width determined directly from the periods, temperatures, and apparent magnitudes of the RR Lyrae variables themselves.

The horizontal branch in 47 Tuc shows the largest intrinsic width of any cluster yet observed. All *C-M* diagrams obtained for this cluster to date show a spread for its HB of at least 0.5 mag, beginning with the discovery paper by Wildey (1961), where the unique nature of the entire *C-M* diagram was first discussed, and continuing with the recent measurements of Lee (1977*b*) and of Hesser *et al.* (1987). The substantial number of stars which can be observed in a complete sample of 47 Tuc permits a good mapping of the structure of the vertical spread in this cluster.

A *C-M* diagram is shown in Figure 14 which illustrates details. The data are from measurements of two sets of eight plates in each color. One set of four plates in each color was taken with the Australian 1 m reflector of the Mount Stromlo and Siding Spring Observatories at Siding Spring; the other set was taken with the Swope 1 m reflector at Las Campanas. The measurements from these 16 plates are combined for the 1500 program stars in Figure 14.

The details of this large program have not been published. The evident scatter of those parts of the giant branch that are fainter than $V = 14$ show that our measurements have larger errors than those in the undoubtedly superior photometry of Lee (1977*b*) that appeared at the time when the Australian plus Las Campanas study was completed, making its publication generally unnecessary. Nevertheless, the measuring error of $\sigma(V) \sim 0.02$ mag in our final catalog of 47 Tuc *is* small enough to have a negligible effect on the derived vertical structure of the HB, which is the point of interest here. Since our sample is complete within an annulus, and since there are many more stars than in the catalogs of Lee and of Hesser *et al.*, we discuss it here.

The most significant feature of Figure 14 is the *sharp lower edge* to the HB distribution. Clearly, this edge defines the zero-age horizontal branch. The distribution perpendicular to the lower boundary is non-Gaussian, the steep rise starting at the ZAHB lower edge as expected from theory. In addition, there appears to be a second, brighter sequence leading to the asymptotic giant branch (AGB), separated from the main body of the HB. The *total* vertical magnitude range of the 47 Tuc HB between colors by $B-V$ of 0.5 and 0.9 is $\Delta V = 1.0$ mag, which includes the brighter, separate sequence on the way to the AGB, assuming it is real. The height of the *main body of the HB* is $\Delta V = 0.7$ mag, relative to the level of the ZAHB, adopted to be $V = 14.20$, as shown at the foot of Table 13. The detailed data on the distribution of the 47 Tuc HB stars, found by counting the catalog that produced Figure 14, are listed in column (2) of Table 13, set out in 0.05 mag bins. The standard deviation of the 47 Tuc distribution, calculated from these data, is 0.148 mag. The data are plotted in the top panel of Figure 15.

Similar data on the distribution of HB stars in other clusters, including their variables, are listed in the remaining columns of Table 13, obtained by counting in the photometric catalogs of each cluster previously discussed. The data for NGC 6171 are from counts in Table II of Dickens and Rolland (1972) for HB stars bluer than $B-V = 1.1$, including the RR Lyrae stars from Dickens (1971). The data for NGC 6712 are from counts in the catalog of Cudworth (1988) for HB stars with $B-V$ colors between 0.4 and 1.2, including the variables from the data in Table 11 in the preceding section. The counts in the HB of NGC 6723 in column (5) of Table 13 were made from the catalog by Menzies (1974, his Table III), including the variables from Table 10 here. The crowding corrections given there were made before the count was done. All HB stars in these two lists between $B-V$ colors of 0.00 and 0.70 were counted.

The HB of NGC 362 from the photometry of Harris (1982) is similar to that of 47 Tuc, with a stubby red HB and a scattering of a few stars blueward of the RR Lyrae strip. Also as in 47 Tuc, the sharp lower bound to the HB defines the ZAHB, which occurs at $V = 15.50$. Counts made in Table 5 of Harris of all HB stars bluer than $B-V = 0.73$ are listed in column (6)

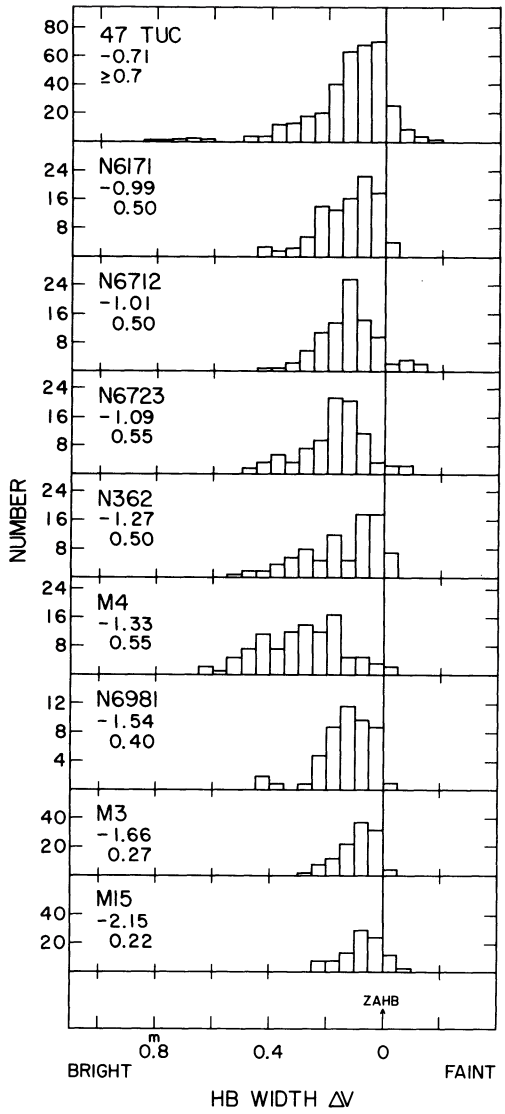

FIG. 15.—Histogram of the horizontal-branch luminosity functions for clusters of different metallicity. The data are from Table 13. The clusters are ordered by metallicity. The [Fe/H] values and the adopted HB width are shown in the code below the cluster name.

of Table 13 and are shown in the fifth panel of Figure 15. Again the steep rise of the distribution and its asymmetric falloff toward brighter magnitudes are evident. The total width of the NGC 362 HB is large at about $\Delta V = 0.5$ mag; the standard deviation of the data in Table 13 is 0.111 mag, as set out at the foot of the table.

The data for M4 in column (7) of Table 13 are seen from counts in Table 3 of Lee (1977*a*) for the obvious HB stars, excluding Lee's data for the RR Lyrae stars. The variables are included in the count by using their mean V-magnitudes from Table 9 in the last section. The total width of the M4 HB is $\Delta V = 0.55$ mag; the standard deviation is 0.135 mag. No sharp lower bound is evident in the distribution, either in Figure 15 or in the *C-M* diagram of Alcaino and Liller (1984), contrary to expectation, presenting an unsolved problem.

Counts of the HB stars in NGC 6981, listed in column (8) of Table 13, have been made in the catalog of Dickens (1972, Table II) after the crowding corrections, previously described, were applied. The variable stars are included, using the data from Table 7 above. The standard deviation, listed at the bottom of Table 13, is 0.097.

The data for M3 and M15, found from counts in Tables 1, 2, 5, and 6, are given in columns (9) and (10) of Table 13. The horizontal branches of these clusters are the narrowest of those listed, showing standard deviation values of ~ 0.07 mag.

No data are given in Table 13 for NGC 3201 because of the complication in defining the fiducial position of the sloping ZAHB in the *C-M* diagram. The lower envelope to the observed HB in the photometry of Lee (1977*c*) has a continually varying slope, which makes the decision of which proper magnitude deviation ΔV to use in the counts somewhat arbitrary. However, the average intrinsic width of the HB can be read from Lee's *C-M* diagram itself to be $\Delta V = 0.30$ mag.

The distributions in Table 13 are plotted in Figure 15 in the order of the metallicity listed by Zinn and West (1984, Table 6). The common feature of most of these distributions is their asymmetry toward brighter magnitudes, presumably due to the progressive shortening of the time intervals along the evolutionary tracks of the post–ZAHB helium shell burning evolutionary phases on the way to the AGB, most of the time being spent near the ZAHB.

The second noteworthy feature of Figure 15 is the variation of the HB width with metallicity. The high metal abundance clusters (47 Tuc, NGC 6171, NGC 6712, NGC 6723, NGC 362, and M4) have intrinsically wide HBs with total ranges of $\Delta V \sim 0.5$ mag, narrowing to about 0.2 mag at M15.

Other clusters of known metallicity with well-determined *C-M* diagrams can be added to the sample to test the generality of the result. The total width of the HB of M5 from the *C-M* diagram of Arp (1955, 1962) and of Buonanno, Corsi, and Fusi Pecci (1981) is $V = 0.35$ mag. The *C-M* diagram for M92 (Sandage and Walker 1966, Figs, 3 and 4; Sandage 1969, Fig. 4) shows a narrow HB width of $\Delta V = 0.25$ mag. The cluster with the lowest known metallicity is NGC 5053 (Zinn and West 1984), which also has the narrowest HB of $\Delta V \sim 0.2$ mag determined from its *C-M* diagram (Sandage, Katem, and Johnson 1977, Fig. 1) using stars on both the blue and red of the RR Lyrae strip.[5]

[5] Anticipating the argument made in the following paper concerning the Oosterhoff effect, we note here the importance of NGC 5053 for understanding the two Oosterhoff period groups (i.e., the period dichotomy). Although NGC 5053 has the lowest metallicity yet measured, it has stars both blueward and *redward* of the RR Lyrae strip. This is in contrast to the rule, followed by most clusters with metallicities between [Fe/H] = −0.7 and −1.6, that the HB color distribution moves progressively (monotonically) blueward as [Fe/H] decreases (cf. Caputo 1985 for a review). But this blueward progression is most pronounced in clusters in the *intermediate range of metallicities* between [Fe/H] = −1.3 and −1.6 such as M13, NGC 2808 (Harris 1974, 1975, 1978), and NGC 6752 (Gascoigne and Ogston 1963; Alcaino 1972; Cannon and Stobie 1973; Wesselink 1974; Cannon 1981), which have horizontal branches that are so blue that they do not intersect the RR Lyrae instability region. In the even lower metallicity clusters with [Fe/H] < −1.6, such as M3, M92, M15, and NGC 5053, the HB again intersects the instability strip, again producing RR Lyrae variables. This reversal (i.e., the nonmonotonic behavior of the HB morphological trend with metallicity) provides the natural explanation of the Oosterhoff period dichotomy. The separation into the two Oosterhoff *period groups* is, then, due to a combination of (1) the relative absence of variable stars in clusters of *intermediate* metallicity (because the HB is not well populated in the variable star strip) together with (2) the dependence of the period on the luminosity, which, as we show in the next paper, depends on the metallicity of the HB. Because no RR Lyrae stars exist in clusters in the metallicity range of [Fe/H] between −1.3 and −1.6, there are no mean periods that are produced by HB luminosities in this metallicity range. This explanation of the Oosterhoff period dichotomy is due to Renzini (1983) and to Castellani (1983). It follows directly from Renzini's Fig. 1 combined with the dependence of RR Lyrae luminosity on metallicity (SKS; S81*b*, S82; Sandage 1990).

TABLE 13

FREQUENCY DISTRIBUTION OF MAGNITUDE DIFFERENCES FROM THE ZAHB

V (1)	47Tuc (2)	N6171 (3)	N6712 (4)	N6723 (5)	N362 (6)	M4 (7)	N6981 (8)	M3 (9)	M15 (10)
-0.20 to -0.16	1	--	--	--	--	--	--	--	--
-0.15 to -0.11	3	2	--	--	--	--	--	--	--
-0.10 to -0.06	9	3	2	--	--	--	--	--	--
-0.05 to -0.01	25	4	2	2	7	2	1	4	11
0.00 to 0.04	70	18	9	3	18	3	9	31	25
0.05 to 0.09	68	23	14	11	18	5	10	37	30
0.10 to 0.14	63	17	26	20	5	5	12	22	14
0.15 to 0.19	40	13	14	21	12	17	9	12	9
0.20 to 0.24	19	14	11	9	5	12	5	7	9
0.25 to 0.29	18	6	6	7	8	14	1	1	
0.30 to 0.34	13	3	3	3	6	12	0		
0.35 to 0.39	12	2	1	5	4	7	1		
0.40 to 0.44	4	3	1	3	2	11	2		
0.45 to 0.49	4		1	2	7				
0.50 to 0.54	0			1	5				
0.55 to 0.59	0			1					
0.60 to 0.64	2			2					
0.65 to 0.69	3								
0.70 to 0.74	2								
0.75 to 0.79	1								
0.80 to 0.84	1								
V of ZAHB	14.20	15.78	16.40	15.70	15.50	13.65	17.10	15.75	15.8 to 16.0
SD(mag)	0.148	0.105	0.107	0.111	0.151	0.135	0.097	0.064	0.072

Figure 16, plotted from the data in Table 14 and Figure 15, shows the correlation of the total widths with [Fe/H]. All clusters except ω Cen follow a trend with little dispersion. However, the deviation of this cluster from the general correlation is well understood, based on the wide variation of [Fe/H] among the individual ω Cen stars. Gratton, Tornambè, and Ortolani (1986) show that the extreme width of the ω Cen HB is undoubtedly caused by a combination of (1) the luminosity spread due to the evolution away from the ZAHB (the effect that is being discussed in this paper) and (2) the variation of the luminosity level of the ZAHB with [Fe/H] (the subject of the paper that follows). Hence, the deviation of ω Cen in Figure 16 is not anomalous. It is expected, based on the arguments we are making here concerning the spread in RR Lyrae luminosities from these two causes, which, while not present in the other clusters, in concert cause a double effect in ω Cen.

Figure 16 shows that the HB width becomes larger for higher metallicities, reaching $\sim$0.6 mag at [Fe/H] = -1.0. It is not clear whether the available theoretical evolution models are consistent with this result. Although the width of the theoretical HB from the model tracks does depend on helium because of the nature of the tracks in their initial departure from the ZAHB at a given [Fe/H] value (cf. SG, Figs. 1–5) there is no sensitivity of the track widths to variations of [Fe/H] at constant He and core mass (cf. Figs. 1 and 4 of SG at any given Y-value). Note also that there is no difference in the width of the tracks for different [Fe/H] at fixed core mass and

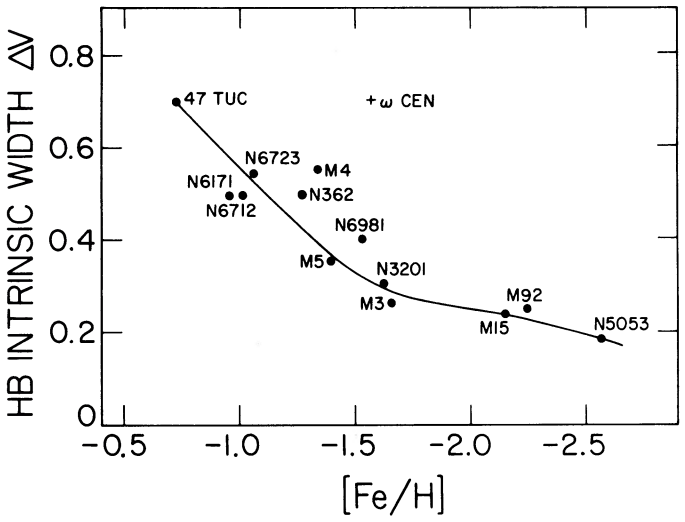

FIG. 16.—Variation of the intrinsic HB width with metallicity from data in Table 14.

TABLE 14

WIDTH OF HORIZONTAL BRANCH AS A FUNCTION OF METALLICITY

Cluster (1)	[Fe/H] (2)	$\langle P_{ab} \rangle$ (3)	ΔV (4)
NGC 5053	−2.58	0.672	0.19
M92	−2.25	0.626	0.25
M15	−2.15	0.640	0.22
M3	−1.66	0.551	0.27
NGC 3201	−1.61	0.558	0.30
ω Cen	−1.59	0.653	0.70
NGC 6981	−1.54	0.552	0.40
M5	−1.40	0.547	0.35
M4	−1.33	0.538	0.55
NGC 362	−1.27	0.542	0.50
NGC 6723	−1.09	0.540	0.55
NGC 6712	−1.01	0.557	0.50
NGC 6171	−0.99	0.527	0.50
47 Tuc	−0.71	...	0.70

the Y-values there (cf. Figs. 2 and 5 of SG). One way in which Figure 16 can be explained is with the model of Lee, Demarque, and Zinn (1988, 1990), mentioned earlier, where the lowest metallicity clusters have no stars on the *ZAHB* in the RR Lyrae gap and redward from it. Stars that are in the instability region have all evolved redward on tracks that funnel into a narrow luminosity range near the endpoints of the evolution just before rising toward the AGB. This morphology does give a narrower HB width for metal-poor stars than for metal-rich ones. However, the difficulty with these precepts is that the expected mass of the HB stars in metal-poor clusters is modeled by LDZ to be *smaller* than the "observed" mass of RR Lyrae stars of a given metallicity that is obtained from the observed period ratios of double-mode RR Lyraes (cf. the discussions on this point in the two papers that follow, where, however, it is pointed out that the theory of the double-mode masses has not yet been done for an appropriate range of metal abundances; see also Lee, Demarque, and Zinn 1990). There is, then, as yet no theoretical understanding of Figure 16 (on the assumption that there is a mass difficulty with the LDZ model, permitting it to be set aside for the moment), perhaps signaling (by Bondi's advice to observers that where there is conflict between theory and observation, it is usually the observations that are wrong) that the validity of the diagram itself needs to be verified.

VIII. SUMMARY

1. The absolute magnitudes of RR Lyrae stars at a given temperature in a given cluster show total intrinsic spreads, presumably due to post–ZAHB evolution, that vary between 0.2 and 0.5 mag for metallicities [Fe/H] between -0.7 and -2.2. The spread increases with higher metallicities. Standard deviations of the magnitude spread within the HB vary from 0.15 mag for 47 Tuc to 0.06 mag for M3, M15, and NGC 5053. The distribution of magnitude residuals is usually non-Gaussian, being steep on the faint side at the ZAHB, with a long tail on the bright side, in agreement with expectations of the evolutionary tracks. Evidently, most of the HB lifetime is spent near the ZAHB rather than on tracks away from it.

2. This finite width of the RR Lyrae star luminosity function at a given period complicates distance determinations to galaxies using such stars when the RR Lyraes are found near the limit of detection. It also complicates the proposed test of the change of zero point of the long-period type I Cepheid P-L relation as a function of [Fe/H]. This test is to be made (A. Saha and J. G. Hoessel 1989, private communication) by comparing apparent magnitudes of Cepheids and RR Lyrae stars in the same galaxy (such as M31 and IC 1613) in order to find the zero-point differences between these two classes of variables in galaxies of different metallicity. Clearly, with the finite luminosity function of the RR Lyrae stars, any survey for the short-period variables must sample deeply enough in apparent magnitude to measure (*a*) the total apparent magnitude spread of the HB due to the effect in Figure 16 caused by evolution, and (*b*) the Oosterhoff period-magnitude-[Fe/H] spread between RR Lyrae samples of different [Fe/H] (S81*a*, *b*; S82).

3. In calibrations of $\langle M_V(\mathrm{RR})\rangle$ by any method, it is necessary to specify whether the values that are obtained in that calibration apply to the unevolved ZAHB variables or to the mean of a given RR Lyrae sample at a given metallicity. These two mean values will differ as a result of luminosity evolution away from the ZAHB.

It is a pleasure to acknowledge conversations and correspondence concerning this paper with C. Cacciari, A. Sweigart, A. Saha, R. Zinn, and an unknown referee. It is also a pleasure to thank Y.-W. Lee, P. Demarque, and R. Zinn for supplying tables of their adopted temperature and bolometric corrections as functions of metallicity and surface gravity that have been used in § III.

APPENDIX A

PERIOD SHIFTS RELATIVE TO THE M3 ZAHB DETERMINED FROM THE PERIOD-AMPLITUDE RELATION

Period shifts at *constant amplitude* were used in earlier demonstrations (S81*a*, *b*) that the RR Lyrae stars have a spread in M_V in a given cluster. The justification for using amplitude rather than temperature as the independent variable in the period correlations is that amplitude is observed to be a unique function of position in the instability strip in any given cluster, albeit with scatter. This scatter, of course, contains the period-shift information which we seek. The advantage of using amplitudes is that such data are more abundant and are generally more precise than color data for cluster variables.

However, use of amplitudes in the problem has been criticized by Caputo (1988). She has suggested that the amplitude at a given color for RR Lyrae stars in ω Cen depends on metallicity and therefore that the period shifts *between* clusters of different metallicities, determined from period-*amplitude* relations relative to M3, are systematically incorrect. A similar criticism has been made by Lee, Demarque, and Zinn (1988, 1990) concerning the use of rise time rather than amplitude for the same purpose. However, these criticisms do not apply to the use of amplitude rather than temperature as the independent variable to find the "period defect" (i.e., the period shift) for individual stars *in a given cluster* where the metallicity is fixed.

The chief advantage of using amplitudes is, of course, that they are independent of reddening, and are therefore particularly important in addressing the question of whether differential reddening can be partly responsible for the correlation of ΔV and $\Delta \log P$ in diagrams such as panels *b* of Figures 9–13, as discussed in footnote 4. The purpose of this appendix is to formulate the main argument of this paper using amplitude rather than temperature data, thereby avoiding the differential reddening problem.

To calculate period shifts from amplitudes, we refer all period shifts to the same fiducial *period-amplitude* relation by adopting the envelope line to the period-amplitude data of M3 listed in Table 5, shown in the upper right-hand panel of Figure 17. The envelope line that is drawn there has the equation

$$\log P = -0.129 A_B - 0.135 . \quad \text{(A1)}$$

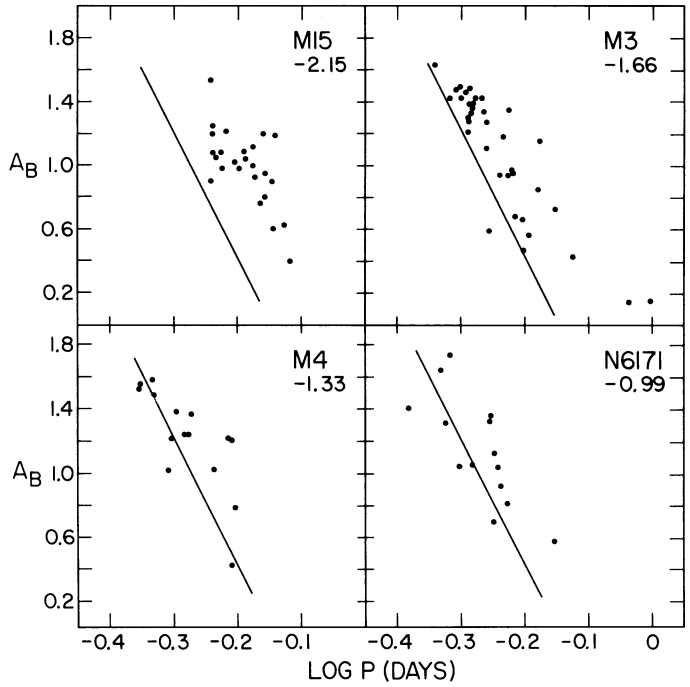

FIG. 17.—Period-amplitude relations for four representative clusters. The line is the adopted lower envelope to the M3 distribution as $\log P = -0.129A_B - 0.135$. This envelope is adopted as the fiducial for all clusters from which to calculate the $\Delta \log P(A_B)$ period shift at constant amplitude. The clusters are ordered by the adopted metallicity shown in the code below the cluster name. Note the progressive shift of the lower envelope of the data toward shorter periods as the metallicity increases. This is the period-shift–metallicity relation for the ZAHB, provided that stars on the lower envelope are, in fact, unevolved.

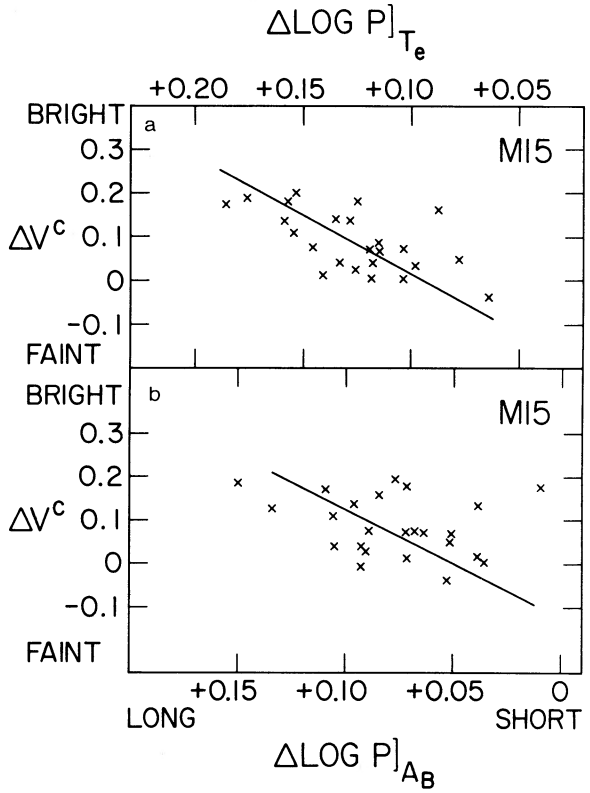

FIG. 18.—Comparison of the correlations between magnitude scatter and the period shifts determined (*a*) at constant temperature and (*b*) at constant amplitude for M15 from data in Table 6.

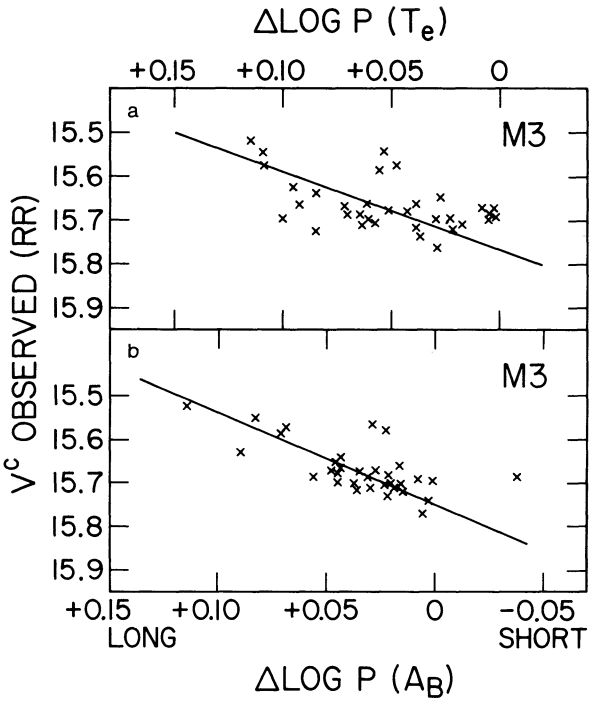

FIG. 19.—Same as Fig. 18, but for M3 from data in Table 5

This M3 line is repeated in the other three panels of Figure 17, where the data from Tables 6, 8, and 9 for M15, NGC 6171, and M4 are plotted. The clusters are placed in the order of their metallicity. Note that this also orders them by the progressive deviation of the points from the M3 envelope line. This, then, is the expression of the period-shift (at constant amplitude)–metallicity relation *between clusters* for the ZAHB, which is the subject of the paper that follows (Sandage 1990). The period shift of any given variable in any *particular* cluster is defined as the difference between the log of the observed period and the log of the period calculated from equation (A1) using the observed amplitude. These "period shifts at constant amplitude," $\Delta \log P(A_B)$, are listed in the antepenultimate or penultimate column in Tables 5–12.

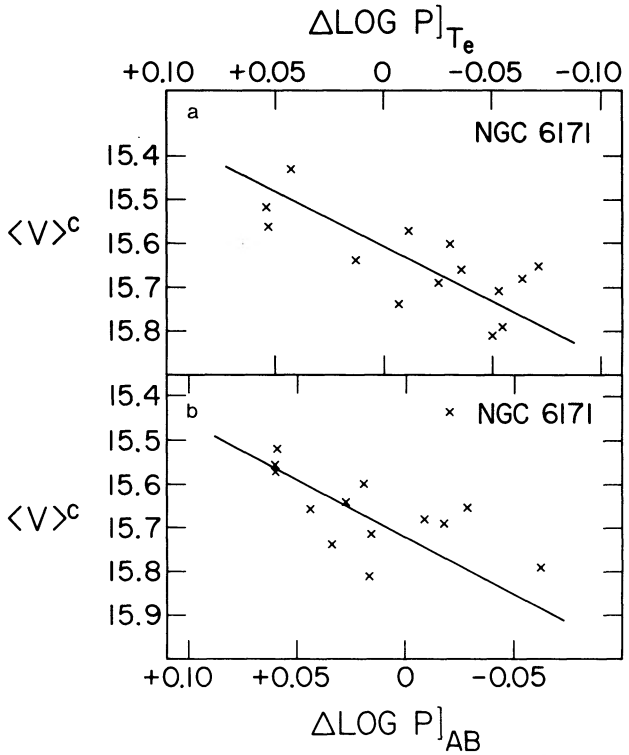

FIG. 20.—Same as Figs. 18 and 19, but for NGC 6171 from data in Table 8

We now inquire whether these period shifts at constant amplitude are as well correlated with the observed RR Lyrae apparent magnitudes as are the $\Delta \log P(T_e)$ values plotted in panels *b* of Figures 9–13. Examples of the correlations using the constant-amplitude period shifts are shown in panels *b* of Figures 18–20 using the data in Tables 6, 5, and 8, respectively, for M15, M3, and NGC 6171. For comparison the correlations are shown again in panels *a* using the constant-temperature period shifts.

The slope of the correlation in Figure 18*b* for M15 is $d\ \Delta V/d\ \Delta \log P(A_B) = 2.52$, with a correlation coefficient of $r = 0.54$, compared with a slope of 2.69 with $r = 0.60$ in the top panel. For the M3 data in Figure 19, Figure 19*a* gives a slope of 1.77 with $r = 0.56$ as in Figure 9 of the text, compared with a slope of 2.12 with $r = 0.83$ in Figure 19*b* [note the better correlation here with $\Delta \log P(A)$ than with $\Delta \log P(T_e)$]. In Figure 20 for NGC 6171 the slopes are similar at 2.55 and 2.51 in Figures 20*a* and 20*b* with correlation coefficients of 0.73 and 0.66, respectively. Clearly, the period shifts at constant temperature and at constant amplitude show the same phenomenon in a given cluster with closely the same slopes for the effect. Differential reddening is, then, clearly not a problem in Figure 16.

APPENDIX B

DATA FOR RR LYRAE STARS IN OMEGA CENTAURI

The position of ω Cen in Figure 16 is anomalous. The observed width of its HB is 0.4 mag larger than the intrinsic HB width of other clusters of similar (mean) metallicity. As mentioned in the text, this increased width is suspected to be due to (1) the effect of the evolution away from the ZAHB discussed in the present paper, combined with (2) the luminosity spread due to the change of the luminosity level of the ZAHB with metallicity, set out in the following paper (Sandage 1990). Because of the combination of these two effects in ω Cen, where there is a variation of [Fe/H] among the stars, the RR Lyrae stars in this cluster give conflicting signals when either effect is looked for separately. The confusion concerning the $M_V = f$[Fe/H] question using ω Cen as a test case has occurred in the past by mixing the two problems. The solution just described, put forward by Gratton, Tornambè, and Ortolani (1986, hereafter GTO 86; Figs. 7 and 8), seems satisfying in all its particulars.

The ω Cen data are listed in Table 15, based on the discussion of Butler, Dickens, and Epps (1978). The "static star" colors in column (7) are from the $\langle B\rangle - \langle V\rangle$ colors in column (6), corrected for amplitude effect by Figure 5. The assumed reddening is $E(B-V) = 0.11$ mag. The other columns are generally self-explanatory.

The period-amplitude relation from these data is shown in Figure 21. The wide scatter is exceptionally well correlated with the apparent magnitude of the particular variable star, leading directly to the formulation of the period-luminosity-amplitude relation, which is equivalent to the period-luminosity-temperature relation (S81*a*, Fig. 3*a*), which is simply an expression of the pulsation condition.

The period shifts at constant amplitude of all ω Cen variables are calculated from the M3 envelope line taken as fiducial, using equation (A1) of Appendix A. The period shifts relative to this line, listed in column (10) of Table 15, are plotted in Figure 22*b* against the bolometric magnitudes listed in column (12). The slope of the correlation is $dm_{\rm bol}/d\ \Delta \log P(A_B) = 2.33$, similar to the data for the other clusters discussed in § VI. The correlation coefficient is high at $r = 0.82$. Note again that the range of the RR Lyrae magnitude is large at 0.7 mag, and that the correlation exists over the entire range of magnitude. Evidently, the combination of post–ZAHB evolution and the variation of the luminosity level of the ZAHB with metallicity produces the large range (GTO 86).

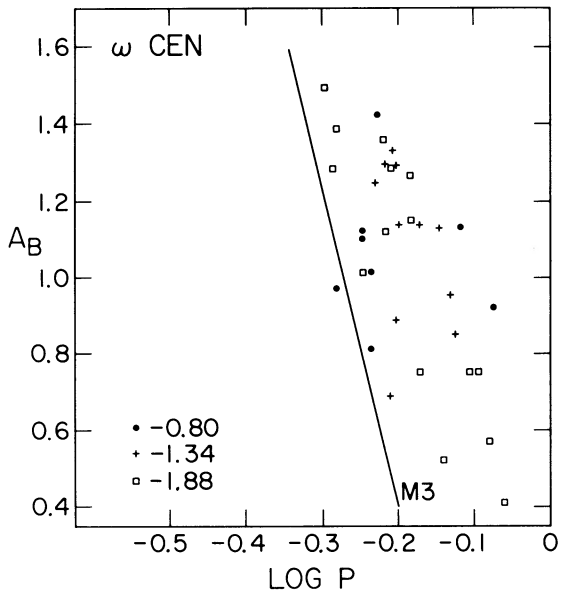

FIG. 21.—Period-amplitude relation for variables in ω Cen from data in Table 15. The M3 fiducial line from Fig. 17 is shown. The variables have been divided into three metallicity bins whose mean values of [Fe/H] are indicated.

TABLE 15

PHOTOMETRIC PARAMETERS FOR RR LYRAE STARS IN ω CEN

Star (1)	log P (2)	A_B (3)	[Fe/H] (4)	<V> (5)	[<B>-<V>]^o E=0.11 (6)	$(B-V)^o_{st}$ (7)	$\log T^{a)}_{e,st}$ (8)	$\log L/M^{0.81}$ (9)	$\Delta\log P(A)^{b)}$ (10)	$\Delta\log P(T_e)^{c)}$ (11)	m_{bol} (12)
				-0.5>[Fe/H]>-1.1; <[Fe/H]>=-0.80							
3	-0.075	0.92	-1.06	14.36	0.37	0.38	3.815	2.029	0.179	0.218	14.33
9	-0.281	0.97	-0.75	14.75	0.28	0.29	3.852	1.937	-0.021	0.148	14.68
44	-0.246	1.12	-0.87	14.64	0.24	0.26	3.860	2.012	0.033	0.213	14.57
55	-0.235	1.01	-0.89	14.77	0.32	0.33	3.840	1.942	0.030	0.150	14.72
67	-0.248	1.10	-0.58	14.66	0.31	0.33	3.840	1.926	0.029	0.137	14.59
84c	-0.237	0.81	-0.51	14.28	0.35	0.35	3.834	2.069	0.132	0.256	14.22
99	-0.116	1.13	-1.04	--	--	--	--	--	0.165	--	
125	-0.227	1.42	-0.69	14.59	0.21	0.26	3.860	2.034	0.091	0.232	14.51
				-1.1>[Fe/H]>-1.6; <[Fe/H]>=-1.34							
4	-0.203	1.29	-1.29	14.52	0.25	0.29	3.842	1.988	0.098	0.189	14.46
7	-0.149	1.13	-1.59	14.47	0.32	0.34	3.822	1.972	0.134	0.171	14.43
13	-0.174	1.14	-1.53	14.44	0.29	0.31	3.832	1.981	0.108	0.181	14.39
27	-0.211	0.69	-1.16	--	--	--	--	--	0.013	--	--
32	-0.207	1.33	-1.17	14.42	0.30	0.34	3.824	1.909	0.100	0.119	14.37
34	-0.134	0.95	-1.22	14.49	0.33	0.34	3.824	1.996	0.124	0.192	14.45
45	-0.230	1.25	-1.14	14.50	0.27	0.30	3.839	1.944	0.066	0.151	14.44
64c	-0.463	0.57	-1.43	14.56	0.23	0.23	3.860	--	--	--	14.49
77c	-0.371	0.48	-1.49	14.49	0.28	0.28	3.843	--	--	--	14.44
79	-0.216	1.30	-1.40	14.62	0.25	0.29	3.839	1.960	0.087	0.165	14.56
83c	-0.448	0.57	-1.58	14.57	0.22	0.22	3.863	--	--	--	14.50
85	-0.129	0.86	-1.16	14.49	0.31	0.32	3.833	2.039	0.117	0.230	14.44
95c	-0.393	0.49	-1.36	14.48	0.30	0.30	3.836	--	--	--	14.43
96	-0.204	0.89	-1.28	--	--				0.046	--	
124c	-0.479	0.60	-1.45	14.56	0.18	0.18	3.876	--	--	--	14.48
				-1.6>[Fe/H]>-1.3; <[Fe/H]>=-1.88							
5	-0.288	1.28	-2.13	14.82	0.28	0.32	3.823	1.808	0.012	0.034	14.78
8	-0.283	1.39	-1.75	14.62	0.20	0.24	3.853	1.939	0.031	0.031	14.55
10c	-0.426	0.52	-1.65	14.52	0.21	0.21	3.864	--	--	--	14.45
14c	-0.424	0.61	-2.09	14.55	0.21	0.21	3.861	--	--	--	14.49
18	-0.206	1.29	-1.76	14.49	0.31	0.35	3.814	1.869	0.095	0.083	14.44
22c	-0.402	0.54	-2.23	14.51	0.26	0.26	3.844	--	--	--	14.47
33	-0.220	1.36	-2.18	14.52	0.30	0.34	3.814	1.852	0.090	0.069	14.49
36c	-0.420	0.55	-1.85	14.48	0.24	0.24	3.850	--	--	--	14.42
38	-0.108	0.75	-1.69	14.52	0.36	0.36	3.811	1.973	0.124	0.170	14.50
39c	-0.405	0.56	-2.14	14.55	0.19	0.19	3.868	--	--	--	14.49
49	-0.219	1.12	-1.93	14.57	0.36	0.38	3.798	1.787	0.060	0.011	14.56
56	-0.246	1.01	-1.64	14.75	0.33	0.34	3.822	1.854	0.019	0.072	14.72
57	-0.100	0.75	-1.80	14.48	0.35	0.35	3.810	1.978	0.132	0.174	14.45
63	-0.083	0.57	-1.98	14.50	0.35	0.35	3.810	1.999	0.126	0.191	14.48
68c	-0.272	0.52	-1.79	14.24	0.26	0.26	3.844	--	0.060	0.258	14.19
69	-0.185	1.15	-1.68	14.56	0.28	0.30	3.836	1.985	0.098	0.185	14.51
72c	-0.415	0.52	-2.18	14.54	0.23	0.23	3.854	--	--	--	14.49
74	-0.298	1.49	-1.80	14.56	0.24	0.29	3.833	1.838	0.029	0.061	14.50
76c	-0.471	0.42	-1.94	14.59	0.15	0.15	3.881	--	--	--	14.52
104	-0.062	0.41	-1.61	14.46	0.34	0.34	3.820	2.065	0.126	0.249	14.43
114	-0.171	0.75	-1.98	--	--			--	0.061	--	
126c	-0.466	0.52	-1.80	14.58	0.19	0.19	3.868	--	--	--	14.51
134	-0.185	1.27	-1.66	14.52	0.27	0.30	3.833	1.972	0.114	0.174	14.47
160c	-0.401	0.52	-1.86	14.55	0.23	0.23	3.854	--	--	--	14.49
163c	-0.504	0.27	-1.92	14.56	0.16	0.16	3.878	--	--	--	14.49

NOTE.—From data listed by Butler, Dickens, and Epps 1978.

[a] Temperatures in col. (8) based on individual [Fe/H] values, listed in col. (4), entered into the color-temperature-metallicity relation.

[b] $\Delta \log P(A)$ in col. (10) is relative to the M3 ZAHB lower envelope of $\log P = -0.129 A_B - 0.135$.

[c] $\Delta \log P(T_e)$ in col. (11) is relative to the M3 ZAHB lower envelope of $\log P = -3.70 \log T_e + 13.823$.

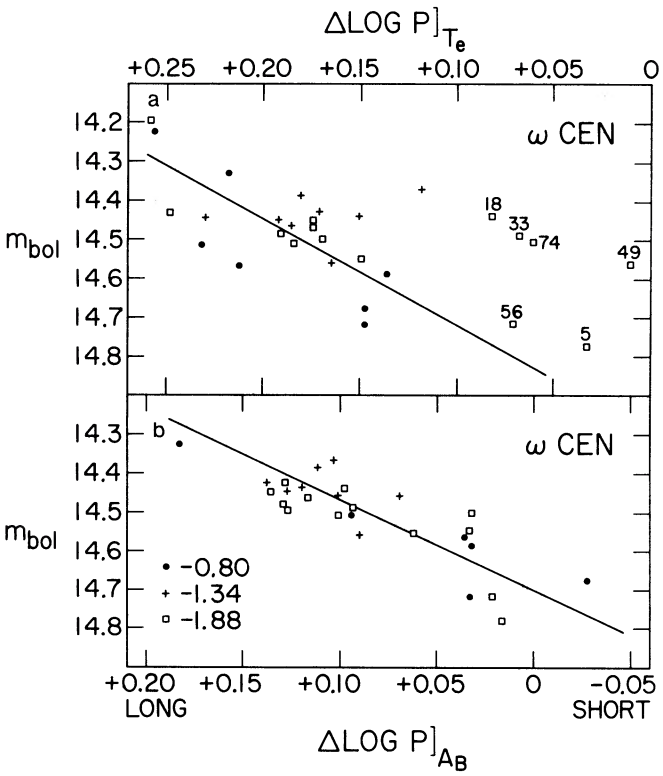

FIG. 22.—Same as Figs. 9–12, but for ω Cen from data in Table 15

The correlation of period shifts at constant temperature, listed in the penultimate column of Table 15, are plotted against the bolometric magnitudes in Figure 22*a*. Deviant points are marked with the star name. With the exception of four stars (Nos. 18, 33, 49, and 74, all in the bin of lowest metallicity), the correlation again is good. Its slope is 2.77, close to the theoretical expectation. Neglecting the four stars, the correlation coefficient is high at $r = 0.81$. At present we have no explanation for the four deviants (other than small errors in the measured colors). New photometry by Dickens and Bingham (in preparation) should test their reality.

REFERENCES

Alcaino, G. 1972, *Astr. Ap.*, **16**, 220.
Alcaino, G., and Liller, W. 1984, *Ap. J. Suppl.*, **56**, 19.
Arp, H. C. 1955, *A.J.*, **60**, 317.
———. 1962, *Ap. J.*, **135**, 311.
Arp, H. C., Baum, W. A., and Sandage, A. 1953, *A.J.*, **58**, 4.
Bingham, E. A., Cacciari, C., Dickens, R. J., and Fusi Pecci, F. 1984, *M.N.R.A.S.*, **209**, 765.
Buonanno, R., Corsi, C. E., and Fusi Pecci, F. 1981, *M.N.R.A.S.*, **196**, 435.
———. 1989, *Astr. Ap.*, **216**, 80.
Butler, D., Dickens, R. J., and Epps, E. 1978, *Ap. J.*, **225**, 148.
Cacciari, C. 1979, *A.J.*, **84**, 1542.
———. 1984, *A.J.*, **89**, 231.
Caloi, V., Castellani, V., and Tornambè, A. 1978, *Astr. Ap. Suppl.*, **33**, 169.
Cannon, R. D. 1981, in *IAU Colloquium 68, Astrophysical Parameters for Globular Clusters*, ed. A. G. D. Philip and D. S. L. Hayes (Schenectady: Davis), p. 501.
Cannon, R. D., and Stobie, R. S. 1973, *M.N.R.A.S.*, **162**, 227.
Caputo, F. 1985, *Rept. Progr. Phys.*, **48**, 1235.
———. 1988, *Astr. Ap.*, **189**, 70.
Caputo, F., Castellani, V., and Wood, P. R. 1978, *M.N.R.A.S.*, **184**, 377.
Castellani, V. 1983, *Mem. Soc. Astr. Italiana*, **54**, 141.
Ciardullo, R. B., and Demarque, P. 1977, *Trans. Yale Univ. Obs.*, Vol. **33**.
Cox, A. N. 1987, in *IAU Colloquium 95, Second Conference on Faint Blue Stars*, ed. A. G. D. Philip, D. S. Hayes, and J. W. Liebert (Schenectady: Davis), p. 161.
Cudworth, K. M. 1988, *A.J.*, **96**, 105.
Dickens, R. J. 1971, *Ap. J. Suppl.*, **22**, 249.
———. 1972, *M.N.R.A.S.*, **157**, 281.
Dickens, R. J., and Flinn, R. 1972, *M.N.R.A.S.*, **158**, 99.
Dickens, R. J., and Rolland, A. 1972, *M.N.R.A.S.*, **160**, 37.
Dorman, B., VandenBerg, D. A., and Laskarides, P. G. 1989, *Ap. J.*, **343**, 750.
Faulkner, J. 1966, *Ap. J.*, **144**, 978.
Faulkner, J., and Iben, I. 1966, *Ap. J.*, **144**, 995.
Gascoigne, S. C. B., and Ogston, F. A. 1963, *Observatory*, **83**, 64.
Gingold, R. A. 1976, *Ap. J.*, **204**, 116.
Gratton, R. G., Tornambè, A., and Ortolani, S. 1986, *Astr. Ap.*, **169**, 111 (GTO 86).
Hachenberg, O. 1939, *Zs. Ap.*, **18**, 49.
Harris, W. E. 1974, *Ap. J. (Letters)*, **192**, L161.
———. 1975, *Ap. J. Suppl.*, **29**, 397.
———. 1978, *Pub. A.S.P.*, **90**, 45.
———. 1982, *Ap. J. Suppl.*, **50**, 573.
Hartwick, F. D. A., Härm, R., and Schwarzschild, M. 1968, *Ap. J.*, **151**, 389.
Hesser, J. E., Harris, W. E., VandenBerg, D. A., Allwright, J. W. B., Shott, P., and Stetson, P. B. 1987, *Pub. A.S.P.*, **99**, 739.
Iben, I. 1971, *Pub. A.S.P.*, **83**, 697.
Iben, I., and Faulkner, J. 1968, *Ap. J.*, **153**, 101.
Iben, I., and Rood, R. T. 1970, *Ap. J.*, **161**, 587.
Lee, S.-W. 1977*a*, *Astr. Ap. Suppl.*, **27**, 374.
———. 1977*b*, *Astr. Ap. Suppl.*, **27**, 381.
———. 1977*c*, *Astr. Ap. Suppl.*, **28**, 409.
Lee, Y.-W., Demarque, P., and Zinn, R. 1988, in *Calibration of Stellar Ages*, ed. A. G. D. Philip (*Van Vleck Obs. Contr.*, No. 7; Schenectady: Davis), p. 149.
———. 1990, *Ap. J.*, **350**, 155.
Menzies, J. 1974, *M.N.R.A.S.*, **168**, 177.
Newell, E. B. 1970, *Ap. J.*, **159**, 443.
Newell, E. B., Rodgers, A. W., and Searle, L. 1969*a*, *Ap. J.*, **156**, 597.
———. 1969*b*, *Ap. J.*, **158**, 699.
Oke, J. B., Giver, L. P., and Searle, L. 1962, *Ap. J.*, **136**, 393.
Oosterhoff, P. Th. 1944, *Bull. Astr. Inst. Netherlands*, **10**, 55.
Preston, G. W. 1961, *Ap. J.*, **133**, 29.
Pritchet, C. J., and van den Bergh, S. 1987, *Ap. J.*, **316**, 517.
Renzini, A. 1983, *Mem. Soc. Astr. Italiana*, **54**, 335.
Roberts, M. S., and Sandage, A. 1955, *A.J.*, **60**, 185.
Rood, R. T. 1970, *Ap. J.*, **161**, 145.
Saha, A., and Hoessel, J. G. 1987, *A.J.*, **94**, 1556.
Sandage, A. 1956, *Ap. J.*, **123**, 278.
———. 1958, in *Stellar Populations*, ed. D. O'Connell (*Ric. Astr.*, **5**, 41).

Sandage, A. 1969, *Ap. J.*, **157**, 515.
———. 1981*a*, *Ap. J.* (*Letters*), **244**, L23 (S81*a*).
———. 1981*b*, *Ap. J.*, **248**, 161 (S81*b*).
———. 1982, *Ap. J.*, **252**, 553 (S82).
———. 1990, *Ap. J.*, **350**, 631.
Sandage, A., and Katem, B. 1982, *A.J.*, **87**, 537 (SK).
Sandage, A., Katem, B., and Johnson, H. L. 1977, *A.J.*, **82**, 389.
Sandage, A., Katem, B., and Kristian, J. 1968 *Ap. J.* (*Letters*), **153**, L129.
Sandage, A., Katem, B., and Sandage, M. 1981, *Ap. J. Suppl.*, **46**, 41 (SKS).
Sandage, A., Smith, L. L., and Norton, R. H. 1966, *Ap. J.*, **144**, 894.
Sandage, A., and Walker, M. F. 1966, *Ap. J.*, **143**, 313.
Sawyer Hogg, H. 1973, *Pub. David Dunlap Obs.*, Vol. **3**, No. 6.
Seares, F. H. 1944, *Ap. J.*, **100**, 255.
Searle, L., and Rodgers, A. W. 1966, *Ap. J.*, **143**, 809.
Seidel, E., Demarque, P., and Weinberg, D. 1987, *Ap. J. Suppl.*, **63**, 917.
Sturch, C. R. 1977, *Pub. A.S.P.*, **89**, 349.
Sweigart, A. V., and Gross, P. G. 1976, *Ap. J. Suppl.*, **32**, 367 (SG).
Sweigart, A., Renzini, A., and Tornambè, A. 1987, *Ap. J.*, **312**, 762.
van Albada, T. S., and Baker, N. 1971, *Ap. J.*, **169**, 311.
Wesselink, A. 1974, *M.N.R.A.S.*, **168**, 345.
Wildey, R. L. 1961, *Ap. J.*, **133**, 430.
Zinn, R., and West, M. 1984, *Ap. J. Suppl.*, **55**, 45.

ALLAN SANDAGE: The Observatories of the Carnegie Institution of Washington, 813 Santa Barbara Street, Pasadena, CA 91101-1292